國立交通大學

機械工程學系

博 士 論 文

燃煤發電廠中排煙脫硫之不透光率研究

Study on in-Stack Opacity Following Flue Gas Desulphurization (FGD) at a Coal-Fired Power Plant

研 究 生：涂文福

指導教授：林振德　教授

中 華 民 國 一 〇 一 年 一 月

燃煤發電廠中排煙脫硫之不透光率研究

Study on in-Stack Opacity Following Flue Gas Desulphurization (FGD) at a Coal-Fired Power Plant

研究生：涂文福　　Student：Wen-Fu Tu

指導教授：林振德　　Advisor：Dr. Jenn-Der Lin

國 立 交 通 大 學

機 械 工 程 學 系

博 士 論 文

A Thesis

Submitted to Department of Mechanical Engineering

College of Engineering

National Chiao Tung University

in partial Fulfillment of the Requirements

for the Degree of

Doctor of Philosophy

in

Mechanical Engineering

January 2012

Hsinchu, Taiwan, Republic of China

中華民國一〇一年一月

燃煤發電廠中排煙脫硫之不透光率研究

學生： 涂文福　　指導教授： 林振德 博士

國立交通大學機械工程學系博士班（熱流組）

中文摘要

燃煤發電廠之排放煙囪內不透光率通常是用來檢測微粒濃度排放量的方法，它是利用光穿透儀，作為一個連續排放監測系統的一部分。然而，安裝排煙脫硫裝置，採用濕式洗滌方法後，濕氣會影響不透光率的測量，水氣產生干擾甚至可能在極低微粒濃度下，不透光率仍超過20%法定上限。本文研究以燃煤電廠(發電量14.3 MW，煙囪直徑為2.4 M，高度為70 M)之排煙溼式脫硫洗滌器對不透光率影響進行實驗與分析。透過實驗調整鍋爐負荷、靜電集塵器和排煙溼式脫硫，以確定在不同狀況下不透光率影響因素的變化量之多寡。研究結果顯示，影響不透光率的兩個重要參數為微粒和水氣消光因子。本文研究不透光率影響因子乃先定義其獨立的質量消光係數 k_p (微粒)與 k_w (水氣)，而利用比爾定律且以非線性迴歸方法計算 k_p 和 k_w 值的變化。結果顯示，k_p 從 0.199 到 0.316 m^2/g 和 k_w 從 0.000345 到 0.000426 m^2/g，其整體平均估計值 k_p 為 0.229 m^2/g、k_w 為 0.000397 m^2/g。雖然 k_w 小於 k_p 3 個數量級，但實驗結果顯示，水氣的消光效應可與微粒的消光效應相比擬，此乃受溼式脫硫洗滌器大量的水氣所影響。理論消

光係數也使用米氏理論加以計算(光學折射率為 1.5－*ni*)，米氏理論所求出的消光係數範圍從 0.282 到 0.286 m^2/g，稍大於平均值 0.229 m^2/g 的實驗消光係數值，其差異原因為粉煤飛灰可能已經形成了以球連著小顆粒或是中空的圓體球形，而非米氏理論的球狀假設。而過去的文獻研究在測定 k_p 值則不考慮水氣的影響以致於高於本文的研究，此乃排煙濕式脫硫之水氣反射所致。除此之外，本文研究結果顯示微粒吸收水氣的影響可以忽略不計。

本研究亦使用敏感度分析不透光率經驗式中各項參數改變時最適切的解及預測某數值有變動時，研究該數值如何變動，以確定不透光率與獨立變量的定量影響。敏感度分析結果表示，不論是微粒質量消光係數或是水氣質量消光係數，若質量消光係數值較大，則對不透明度的影響將隨之變大。最後，根據環保署的微粒物排放限值，我們建立微粒排放濃度與不透光率相關係式，在考慮水氣與二氧化氮的影響下，可得到不透光率為 33.8%時仍能符合微粒排放濃度的限制。本研究中更進一步將水氣、二氧化氮物及氧氣的影響加以校正，在 95%信賴度區間求得不透光度和微粒濃度的經驗關係式，從而提供不透光率監測與實際微粒排放濃度的相互關係。

關鍵詞: 排煙脫硫、不透光率、消光係數、米氏理論、敏感度分析.

Study on in-Stack Opacity Following Flue Gas Desulphurization (FGD) at a Coal-Fired Power Plant

Student：Wen-Fu Tu　　Advisor：Dr. Jenn-Der Lin

Department of Mechanical Engineering

National Chiao Tung University

ABSTRACT

In-stack opacity, which is used as a surrogate for particle concentrations, can typically be measured using in-situ light transmission meters as part of a continuous emission monitoring system (CEMS) for coal-fired power plants. However after installing flue gas desulfurization (FGD) which utilizes a wet scrubbing method, water moisture can affect the measured opacity which may exceed the limitation of 20% even with lower particulate emissions. In this study, numerous experiments are investigated on factors influencing opacity at a 14.3-MW coal-fired power plant with FGD wet scrubbers. The inside diameter of the stack is 2.4 m and the height is 70 m. The factors of in-stack opacity are set with adjusting the boiler load, Electrostatic Precipitator (ESP) and FGD. Experiments are performed to determine variations in opacity for different values of the variables. The results show that two important factors that affect in-stack opacity—light extinction by emitted particles and that by water moisture after a FGD unit—are investigated. The mass light extinction coefficients for particles and water moisture, k_p and k_w, respectively, were determined using the Lambert-Beer law of opacity with a nonlinear least-squares regression method. The estimated k_p and k_w values vary from 0.199 to 0.316 m^2/g and 0.000345

to 0.000426 m^2/g, respectively, and the overall mean estimated values are 0.229 and 0.000397 m^2/g, respectively. Although k_w is 3 orders of magnitude smaller than k_p, experimental results show that the effect on light extinction by water moisture was comparable to that by particles because of the existence of a considerable mass of water moisture after a FGD unit. The mass light extinction coefficient was also estimated using Mie theory with measured particle size distributions and a complex refractive index of 1.5-*ni* for fly ash particles. The k_p obtained using Mie theory ranges from 0.282 to 0.286 m^2/g and is slightly greater than the averaged estimated k_p of 0.229 m^2/g from measured opacity. The discrepancy may be partly due to a difference in the microstructure of the fly ash from the assumption of solid spheres because the fly ash may have been formed as spheres attached with smaller particles or as hollow spheres that contained solid spheres. Previously reported values of measured k_p obtained without considering the effects of water moisture are greater than that obtained in this study, which is reasonable because it reflects the effect of extinction by water moisture in the flue gas. Additionally, the moisture absorbed by particulate matter, corresponding to the effect of water moisture on the particulates, was clarified and found to be negligible.

Sensitivity analyses using a correlation equation are also conducted to determine the quantitative effect of the independent variables on plume opacity. Results on sensitivity analyses illustrate that at larger value of the mass light extinction coefficients of either particles or water moisture, the influence of the exhaust emission on the opacity becomes larger. Finally, we also discuss the opacity according to the particulate emission limit of Environmental Protection Agency (EPA) in Taiwan. Results indicate that the in-stack opacity could increase to 33.8% but still meet the requirement of EPA limit when water moisture is taken into consideration. Further, in

consideration of water moisture, NOx and oxygen calibration, an empirical correlation between opacity and particulate concentration is given with 95% confidence intervals. The results provide useful information concerning the influence of various factors on in-stack opacity and may be utilized for possible modifications in measurements for monitoring particulate emissions by opacity.

Keywords: flue gas desulfurization、opacity、extinction coefficient、Mie theory、sensitivity analyses.

誌　　謝

自從進入交大機械系博士班就讀後，指導老師林振德教授在這段博士班期間即給予適切的引導，幫助我不論是在論文研究或工作上都有清晰的思路。由於老師的教導能讓我以較為嚴謹的邏輯來處理相關的環節，這樣的思考模式相信對於將來在面對問題與解決問題時會有很大的幫助。因此，在此特別感謝論文指導老師，雖然老師您榮任虎尾科技大學校長與交大機械系論文指導老師，相當辛苦與繁忙，但是，在此段博士班求學期間都給予相當充裕的指導與諄諄教誨，終使博士論文得以順利完成任務。

同時感謝論文口試召集人傅武雄副教務長以及口試委員蔡春進教授、林成原教授、吳志陽教授與許隆結副教授對於論文上的指正及建議。也感謝成大環工所吳義林教授與助教邱慧真對於論文的幫忙與協助，使得此論文的研究架構能更加的扎實及明瞭。

我非常珍惜在交大機械系博士班期間的日子，謝謝學長陳志堅、許隆結及學弟賴志銘對於我相關論文的協助與幫忙。特別感謝許隆結學長花費很多時間幫忙提供論文架構思索與校稿，以及學弟賴志銘提供相關論文相關資料的參考與應用，使得博士論文能順利完成。也感謝我目前服務於台灣國際造船公司的上級長官及船裝工場鄭主任與

工程師、領班、班長及現場師傅們給予我在博士班求學時的幫忙，使我不僅能達成公司給予我單船工程師的職責與任務，也能順利完成博士學業，在此真的感謝船裝工場的弟兄，謝謝您們。最後，感謝家人與親戚及拜把兄弟霍萬興的支持與鼓勵，讓我最終能取得交大機械工程學系的博士學位!

Table of contents

List of tables

List of figures

Nomenclatures

A_p : Particle area, [μ m^2]

Conc. $i_{(Std.\ O2)}$: Pollutant concentration at the O_2 level specified in the standard, [%]

Conc. $i_{(Measured\ O2)}$: Pollutant concentration measured in the exhaust stack, [%]

C_{ext} : Scattering cross-section, [$1/m^2$]

C_{abs}: Absorption cross-section, [$1/m^2$]

C_{sca} : Scattering cross-section, [$1/m^2$]

d: particles of diameter, [μ m]

I_{sca}: Intensity of the wave scattered by the angle, [°]

k : mass extinction coefficient, [1/m]

K : Ratio of specific particulate volume to mass extinction coefficient, [cm^3/m^2]

L : Optical path length, [m]

N : Number of moisture droplets per unit volume, [n/m^3]

$Op_{i,e}$: Measured opacity, [%]

$Op_{i,c}$: Estimated opacity, [%]

r : Particle radius, [μ m]

Std. O_2% : O_2 concentration specified in the standard, [%]

W : Mass concentration, [g/Nm^3]

W_p' : Particle mass concentration at 6% O_2, [%]

X_w : Mole fraction of water moisture, [%]

X_{wt} : Theoretical mole fraction of water vapor with the saturated flue gas, [%]

x : Ratio of the meridional circumference of the sphere to the wavelength of light in the medium, [%]

$Y(i)$: Matrix of measured opacity, [%]

ρ : Density of the substance, [g/cm^3]

λ : Wavelength, [μ m]

Ω : Solid angle, [$^\circ$]

$\Phi(\Theta)$: Scattering phase function, [sr^{-1}]

Θ : Wave scattering angle, [rad]

Nondimension

a : Experimental samples

a_n : Mie scattering coefficient

b : Initial guess

b_n : Mie scattering coefficient

E : Square error

$f(r)$: Normalized particle number density

I : Transmitted intensity

I_0 : Incident intensity

I_{in}: Incident unpolarized beam

i: nondimensional polarized intensities

m: Index of refraction

n : Image part of refractive index

Q : Efficiency factor

Q_e: Extinction efficiency factor

Q_s : Scattering efficiency factor

Q_a : Absorption efficiency factor

S: Radiative source function

Sy : Standard error

$S(\Theta)$: Amplitude functions.

t : Appropriate student-t distribution

X : Sensitivity coefficients

π_n : direction-dependent function 1.

τ_n : direction-dependent function 2.

ψ_n : Riccati-Bessel function 1.

ξ_n : Riccati-Bessel function 2.

σ_{ext}: Extinction coefficient

$\eta(\beta)$: Matrix of estimated opacity

$\tilde{\beta}$: Corresponding set of solutions

δ_{kp}: Uncertainty of K_p

δ_{kw}: Uncertainty of K_w

$\Im$: Imaginary part of complex number

Subscripts

i : Contribution of species

p: Particles

w: Water moisture

NO_2: NO_2 emission

SO_x: SO_x emission

1,2: in medium, or at location, “1” or “2”

Chapter 1 Introduction

1.1 Background

The air quality and visibility in an environment are strongly related to the pollutant emissions from industrials in that area. Among industrials, coal-fired furnaces and power plants are major sources of the pollutants. In a coal-fired power plant, in-stack opacity can be typically be measured using in situ light transmission meters as part of a continuous emission monitoring system (CEMS) of the pollutants. Opacity is defined as the percentage of transmitted light that is obscured as it passes through a medium. The obscuration is caused by extinction, which consists of absorption and scattering by constituents in the medium.[1, 2] It is a function of particulate concentrations and many other independent optical and physical variables, such as particle size distribution, particle density, refractive index of particles, and nitrogen dioxide and sulfuric acid concentration in the exhaust gas, as examined in previous studies. The extinction of a constituent is usually expressed in terms of mass extinction coefficient (k),[3, 4] the extinction coefficient (k multiplied by concentration), or the ratio of specific particulate volume to mass extinction coefficient (K).[5–9] In a coal-fired power plant, flue gas desulphurization (FGD) unit is often used to reduce sulfuric acid gas emission. However, after setting the FGD unit, water moisture may affect the opacity measurement. The in-stack opacity is significantly affected by the water moisture after FGD with the wet scrubbing method.

1.2 Literature survey

For experiments on a Kraft mill recovery furnace, Bosch[5] and Larssen *et al.*[6] utilized a bolometer and a smoke meter, respectively, to compare the theoretical and

measured opacities due to particles. The calculated *K* values for 18 tests were in the range of 0.80 –1.20 cm^3/m^2; the variation was due to variations in the size distribution parameters. Thielke and Pilat[7] conducted simultaneous measurements of the in-stack opacity, particle mass concentration, and particle size distribution of a hogged-fuel boiler, a Kraft recovery furnace, and a pulverized coal-fired boiler to assess the validity of the particle mass concentration-opacity relationship. The results of their study indicate the importance of using the actual particle size distribution (particle diameter range of 0.2–10μ m) for predicting the relationship between transmittance and mass concentration. Ensor and Pilat[8] studied the effects of particle size on opacity using the Lambert-Beer law to determine the parameter *K* at a coal-fired power plant. Their results showed that *K* is primarily a function of particle size for particles with radii greater than approximately 0.5μ m and is primarily a function of the refractive index for smaller particles. They also studied the effect of particle size distribution on light transmittance measurements.[9] The ratio of the expected extinction coefficient to the theoretical extinction coefficient was reported to be a function of the log-normal size distribution parameters (geometric mass mean radius and geometric standard deviation) for various detector acceptance angles. Cowen *et al.*[10] measured the fly ash light absorption for coal-fired boilers with the integrating plate method. They analyzed the absorption of fly ash samples from four types of coal-fired power plants with various unit ratings and studied the theoretical modeling of smoke plume opacity. By the integrating plate method, which is defined as comparing the light absorption through a clean blank filter to one with a single layer of aerosol, only absorption is measured and the scattering effect is diminished. Steig and Pilat[11] performed simultaneous measurements of in-stack light transmittance, particle mass concentration, and particle size distribution at a pulverized coal-fired boiler. The

measured values of K, which ranged from 0.68 to 0.90 cm^3/m^2, were consistently lower than the theoretically calculated values because of an assumed particle density of 1 g/cm^3. Conner and Knapp[12] evaluated the particle concentration and light attenuation for coal-fired power plants with electrostatic precipitators (ESPs); the value of K varied from 0.11 to 7.50 cm^3/m^2. Pilat and Ensor[13] measured and calculated the light extinction versus aerosol mass concentration relationship for atmospheric and source emission aerosols. The measured values of K ranged from 0.26 to 0.49 m^3/m^2 and from 0.06 to 0.78 cm^3/m^2 for atmospheric aerosol and individual source emission, respectively.

In addition to the effects due to particles, the emissions of sulfur trioxide (SO_3) were a key component of opacity and acid deposition and need to be low enough to not cause opacity violations and acid deposition.[14] The emission of SO_3 depended on the sulfur content in coal, combustion conditions, flue gas characteristics, and air pollution devices. Pilat and Wilder[15] calculated the effect of the initial water and sulfuric acid (H_2SO_4) concentrations and final gas temperature on the opacity after cooling from an original stack gas temperature at 300°C and found significant effects for initial H_2SO_4 concentrations greater than 5 parts per million (ppm). They further evaluated the effects of particle size and found that H_2SO_4 condensation should have minimal effects on particles greater than 1μ m.[16] Lou *et al.*[17] established an empirical equation similar to Beer's law that was used to predict the plume opacity in terms of the stack diameter and concentrations of particles and total water-soluble sulfates. Meng *et al.*[18] presented a computer simulation model that calculates the opacity due to primary particles emitted from the stack and secondary particles that form (such as SO_3 hydrolyzes to H_2SO_4, hydrochloric acid [HCl], and ammonia [NH3]) in the atmosphere after the release of condensable gases from the stack. Lindau[3] measured

the effect of nitrogen dioxide (NO_2) on the flue gas opacity and demonstrated that for a coal-fired boiler with a NO_2 concentration of approximately 10–50 ppm, the effect is approximately 2–10%. Wieprecht *et al.*[19] concluded that the water droplets within the flue gas after a flue gas desulfurization (FGD) unit were mainly formed via condensation onto fly ash particles. Although mist eliminators for coarse and fine droplets are highly efficient in FGD, some water moisture still remains.

It was found that fly ash consists of a mixture of particles with different chemical compositions and thus different optical properties.[20] Most fly ash particles are spherical and glassy because of the rapid cooling of the molten droplets formed during combustion. And most particles are observed to be highly transparent at visible wavelength, whereas a small fraction (generally unburned carbon or iron oxides) are observed to be entirely opaque. Boothroyd *et al.*[21] measured the light scattering phase functions and asymmetry factors for a sample of fly ash and compared them with Mie theory predictions. The results imply that fly ash could be treated as spherical particles under furnace conditions at which they were well dispersed. The complex refractive index (or optical constants) may be used together with Lorenz-Mie theory to predict the absorption, extinction, and scattering properties of particles under assumption of an equivalent sphere model and vice versa.

1.3 Motivation and objectives

The above literature illustrates that in-stack opacity is strongly correlated with various factors such as particle mass concentration, particle size distribution, particle density as well as the H_2SO_4 and NO_2 concentrations, light scattering and refractive index. The concentration of water moisture increases after a FGD unit with wet scrubbing is installed, but the effect of water moisture on opacity has not been fully

evaluated. Besides, the effect of SOx emission on in-stack opacity was not touched in the literatures. To the author's knowledge, the extinction coefficient of SOx has not been determined. The objective of this study aims to investigate the effect of particle concentration, particle size distribution, particle density, water moisture NO_2 and SOx emissions on opacity so as to provide an empirical correlation between opacity and particulate concentration.

1.4 Research Methodology

In the study presented here, experiments were conducted at a full-scale coal-fired power plant to analyze the effects of particles and water moisture on opacity. The parameters K_p, K_w and K_{SOx} (subscripts p and w denote particles and water moisture, respectively) and the mass extinction coefficients k_p, k_w and k_{SOx} for emitted particles, water moisture and sulfur oxides, respectively, in the flue gas that leaves a FGD unit were determined. The parameters of K_p, K_w and K_{SOx} were determined using nonlinear least-squares regression and Newton's method with the Lambert-Beer equation. To clarify the effect of water on the characteristics of particulates, which subsequently affect the extinction coefficient of particles, particle hygroscopicity was also examined. In addition to the empirical results, this study also estimated the parameters K_p and k_p on the basis of the Mie theory using the computational BHMIE program[22, 23] and existing data of complex refractive index for fly ashes under a spherical particle approximation. The estimations were compared with the experimental results of the study presented here. Finally, a correlation between concentration of particulate matter and opacity for coal-fired power plant is provided using regression estimates in consideration of water moisture, SOx and NOx emissions.

The organization of the remaining part of this dissertation is as follows: in

chapter 2, we give a brief review of light scattering theory and opacity. In Chapter 3, experimental equipment, design and procedures are discussed in detailed. In Chapter 4, we describe the inverse methodology for parameter estimation and sensitivity coefficient for various parameters. Results and discussion are given in Chapter 5. A correlation of opacity empirical model is given in Chapter 6. Finally, some conclusions and future works are drawn in Chapter 7.

Chapter 2 Optical Properties

This study investigates the in-stack opacity formation after flue gas desulfurization at a coal-fired power plant. Opacity is an index of obscuration of transmitted light as it passes through a medium. The obscuration is caused by extinction, which consists of absorption and scattering by constituents in the medium. The light extinction is the sum of the light scattering and light absorption coefficients; therefore, the light extinction is needed for evaluation of its effect on opacity. In this chapter, a brief review of light scattering theory and opacity is introduced.

2.1 Extinction

The light extinction is the sum of scattering and absorption by a particle. The total light extinction is expressed in terms of the extinction cross-section as

$$C_{ext} = C_{abs} + C_{sca} \tag{2.1}$$

where C_{ext} is expressed the scattering cross-section, C_{abs} is expressed the absorption cross-section, C_{sca} is expressed the scattering cross-section.

The efficiency factors Q is used instead of cross-sections, being nondimensionalized with the projected surface of the sphere, and the extinction efficiency Q_e of a particle is the sum of its scattering efficiency Q_s and its absorption efficiency Q_a,

$$Q_{ext} = Q_{abs} + Q_{sca} \tag{2.2}$$

Consider a monodispersed aerosol of N particles per unit volume with an extinction coefficient σ_{tp}:

$$\sigma_{tp} = NA_pQ_{ext} = \frac{\pi Nd^2Q_{ext}}{4}. \tag{2.3}$$

where N is the numerical concentration of particles of diameter d, and A_p is the particle area.

Light scattering theory may be categorized in terms of two theoretical frameworks, the Rayleigh and Mie scattering theories. In general, the scattering light intensity is dependent on the shape and size of particles. The Rayleigh theory is applicable to small spherical particles. There is no particle size limitation in Mie scattering theory. Therefore, Mie theory may be used for describing most spherical particle scattering systems, including Rayleigh scattering. However, due to the complexity of the Mie scattering formulation, Rayleigh scattering theory is generally preferred if applicable.

2.2 Mie scattering theory

A size parameter (x) which is the ratio of the meridional circumference of the sphere ($2\pi r$, where radius = r) to the wavelength (λ) of light in the medium, i.e. $x = 2\pi r/\lambda$. The Mie scattering theory is used for calculating light scattering for spherical particles with size parameter $x < 30$.

The ratio of the intensity between wave scattered through an angle Θ by spherical particle, I_{sca}, and the incident light, I_{in}, is given[24,25,26,27] by

$$\frac{I_{sca}(\Theta)}{I_{in}} = \frac{1}{2}\frac{i_1 + i_2}{x^2}; \tag{2.4}$$

where i_1 and i_2 are the non-dimensional polarized intensities, and they are calculated from

$$i_1(x, m, \Theta) = |S_1|^2, \tag{2.5}$$

and

$$i_2(x, m, \Theta) = |S_2|^2. \tag{2.6}$$

where S_1 and S_2 are amplitude functions. The total amount of energy scattered by one sphere into all directions is

$$Q_{sca} = \frac{C_{sca}}{\pi a^2} = \frac{a^2}{\pi a^2} \int_{4\pi} \frac{I_{sca}}{I_{in}} d\Omega = \frac{1}{x^2} \int_0^{\pi} (i_1 + i_2) \sin\Theta d\Theta \tag{2.7}$$

For the general case of arbitrary values for the complex index of refraction m and the size parameter x, the full Mie equations as expressed by van de Hulst must be employed,

$$S_1(\Theta) = \sum_{n=1}^{\infty} \frac{2n+1}{n(n+1)} [a_n \pi_n(\cos\Theta) + b_n \tau_n(\cos\Theta)], \tag{2.8}$$

$$S_2(\Theta) = \sum_{n=1}^{\infty} \frac{2n+1}{n(n+1)} [b_n \pi_n(\cos\Theta) + a_n \tau_n(\cos\Theta)], \tag{2.9}$$

where π_n and τ_n are related to Legendre polynomials P_n by

$$\pi_n(\cos\Theta) = \frac{dP_n(\cos\Theta)}{d\cos\Theta}, \tag{2.10}$$

$$\tau_n(\cos\Theta) = \cos\Theta \pi_n(\cos\Theta) - \sin^2\Theta \frac{d\pi_n(\cos\Theta)}{d\cos\Theta}, \tag{2.11}$$

The Mie *a* and *b* coefficients are at the heart of the calculation, and that for a sphere of radius r these were given as

$$a_n = \frac{\psi_n'(y)\psi_n(x) - m\psi_n(y)\psi_n'(x)}{\psi_n'(y)\xi_n(x) - m\psi_n(y)\xi_n'(x)}, \tag{2.12}$$

and

$$b_n = \frac{m\psi_n'(y)\psi_n(x) - \psi_n(y)\psi_n'(x)}{m\psi_n'(y)\xi_n(x) - \psi_n(y)\xi_n'(x)}. \tag{2.13}$$

where $n \geqq 1$, $x = 2\pi r/\lambda$, $y = ma$ for a complex refractive index *m*. The functions ψ and ξ are the Riccati-Bessel functions, and that related to the Bessel and Hankel functions[28, 29], the ξ similar to the Hankel functions in that $\xi = \psi - ix$. We shall follow Refs. 28-29, and write

$$\psi_n(z) = \left(\frac{\pi z}{2}\right)^{1/2} J_{n+1/2}(z), \tag{2.14}$$

and

$$\xi_n(z) = \left(\frac{\pi z}{2}\right)^{1/2} H_{n+1/2}(z) \tag{2.15}$$

Provided the wavelength λ of incident light, particle size distribution, and the refractive index of material, substitution of Eq. (2.8) and Eq. (2.9) into Eq. (2.7) gives the Q_{ext} for spherical particles as

$$\mathrm{Q_{sca}}(m,x) = \frac{2}{x^2}\sum_{n=1}^{\infty}(2n+1)\left(|a_n|^2 + |b_n|^2\right) \tag{2.16}$$

Finally, total extinction by a single particle (absorption with the particle, plus scattering into all direction) is related to the real part of the amplitude functions and can be expressed as

$$\mathrm{Q_{ext}}(m,x) = \frac{2}{x^2}\sum_{n=1}^{\infty}(2n+1)\Re\{a_n + b_n\}. \tag{2.17}$$

2.3 Rayleigh scattering theory

Rayleigh scattering[24] is applicable when the radius (r) of the scattering sphere is much smaller than the wavelength (λ) of the incident light. Using Rayleigh scattering when r < 0.01 μm are essentially identical to the rigorous results obtained using Mie theory. In order for Rayleigh scattering to be valid, the size of the particle must be much smaller than the wavelength of the incident radiation, both inside and outside of the particle. If the scattering particles are extremely small, then the size parameter x= $2\pi r/\lambda$ becomes very small.

In the limit of r→0, only the a_1 in Eq. (2.12) and Eq. (2.13) is nonzero, or

$$S_2(\Theta) = S_1(\Theta)\cos\Theta = i\frac{m^2-1}{m^2+2}x^3\cos\Theta \tag{2.18}$$

where m is index of refraction.

The amplitude functions (S_1, S_2) for one polarization is independent of scattering angle Θ. then gives the efficiency factors as

$$Q_{sca} = \frac{8}{3}\left|\frac{m^2-1}{m^2+2}\right|^2 x^4 \tag{2.19}$$

$$Q_{abs} = -4\Im\left\{\frac{m^2-1}{m^2+2}\right\}x . \tag{2.20}$$

The extinction efficiency Q_e is the sum of its scattering efficiency Q_s and its absorption efficiency Q_a. Substitution into Eq. (2.7), then give the extinction efficiency factors as

$$Q_{ext} = \frac{8}{3}\left|\frac{m^2-1}{m^2+2}\right|^2 x^4 - 4\Im\left\{\frac{m^2-1}{m^2+2}\right\}x \tag{2.21}$$

2.4 Opacity

A general relationship can be developed between the light transmittance (T) as it passes a medium of thickness L, the relationship between the transmitted intensity (I) and the incident intensity (I_0). The transmission of light through a volume containing an aerosol is described by the Lambert-Beer law[13]. The law states that considering could be expressed by

$$T = \ln(\frac{I}{I_0}) = -\frac{W}{K\rho}L \tag{2.22}$$

where T is transmission, W is the mass concentration, K is the ratio of the volume of a specific particulate to the mass extinction coefficient (cm^3/m^2), ρ is the density of the substance. K is dependent on the composition, size distribution, relative refractive index, and the beam wavelength.

If one couples Eq. (2.22) with the extinction coefficient described in the previous

section, the following equation can be derived.

$$\frac{I}{I_0} = e^{-\frac{W}{K\rho}L} = e^{-\sigma_{ext}L} \tag{2.23}$$

where σ_{ext} is extinction coefficient.

Eq. (2.23) is the remarkable Lambert-Beer law, which illustrates the light intensity decreasing exponentially with travelled distance. Accordingly, the opacity could be expressed as

$$Opacity = 1 - \frac{I}{I_0} = 1 - e^{-\frac{W}{K\rho}L} = 1 - e^{-\sigma_{ext}L} \tag{2.24}$$

Opacity is the amount of light obscured by particulate matters. The light reflected by objects behind the volume will be attenuated as it travels through the medium due to absorption. The amount of light received is therefore necessarily lower that the amount of light emitted. In-stack opacity can be used as an indicator of changes in performance of particulate control systems. The in-stack opacity can be explained in Fig. 2.1. The transmittance can be related to the opacity by

Opacity (%) = 100 − transmission of light (%) (2.25)

Two types of opacity can be considered as in-stack opacity and out-of-stack opacity. In-stack opacity, which is due to emitted dust, gases (e.g. SO_3、NO_2) and aerosols. Out-of-stack, which is the plume opacity formed after flue gas leaving the stack. For in-stack opacity, the major constituents usually consist of particulate, water moisture, sulfuric acid steam, and NO_2. In the present study, the SO_x concentration is controlled by using liquid MgO in the FGD unit. Because the variation in opacity with a considerable change in SO_x concentration was less than 0.6% and all experiments in this study were performed at a SO_x concentration controlled to within approximately 20–36 ppm, the effect of associated SO_x and liquid H_2SO_4 emissions on plume

opacity is thus neglected.

An empirical correlation equation similar to that of the Lambert-Beer equation is then written as

$$Opacity = 1 - e^{-(W_p k_p + W_w k_w + W_{NO2} k_{NO2} + ...)L} = 1 - e^{-(\frac{W_p}{K_p \rho_p} + \frac{W_w}{K_w \rho_w} + \frac{W_{NO2}}{K_{NO2} \rho_{NO2}} + ...)L} \quad (2.26)$$

where W_p, W_w, and W_{NO_2} denote the mass concentrations of particles, water moisture, and NO_2, respectively, and ρ_p, ρ_w, and ρ_{NO_2} are the densities of particles, water, and NO_2, respectively. The parameters K (cm^3/m^2) and k (m^2/g) are defined as described above for species of particulates, water moisture, and NO_2, respectively.

Nitrogen dioxide has absorption bands in the visible light region and thus affects opacity[3]. Eq. (2.26) thus includes the contributions of light extinction by particulates, water moisture, and nitrogen dioxide in the flue gas. Eq. (2.26) reduces to the classical equation for cases of light extinction by particulates only when NO_2 and water moisture are not included. The parameters of W_p, W_w, W_{NO_2}, ρ_p, ρ_w and ρ_{NO_2} in Eq. (2.26) can be readily obtained from experimental measurements, whereas values of K_p and K_w (or k_p and k_w) need to be determined. According to Lindau[3], $1/(K_{NO_2} \times \rho_{NO_2})$ is the mass extinction coefficient k of NO_2 which was measured to be 3.3×10^{-4} ppm^{-1} m^{-1}. The Eq. (2.26) became as

$$Opacity = 1 - e^{-(\frac{W_p}{K_p \rho_p} + \frac{W_w}{K_w \rho_w} + 0.0003 * W_{NO2} + ...)\ L} \quad (2.27)$$

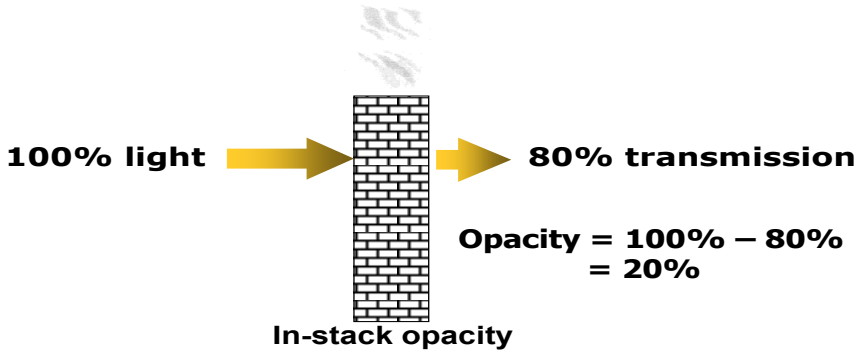

Figure 2.1 The example of in-stack opacity

Chapter 3 Experiments

3.1 Basic information of the power plant in-stack instruments

In the study presented here, experiments were conducted in a commercialized coal-fired power plant with a FGD unit with a wet scrubber, as shown in Figure 3.1. The plant comprises a coal-fired boiler, steam turbines, and a 14.3-MW generator. The FGD unit is downstream of an induced-draft fan (IDF), and an ESP is upstream of the IDF. Exhaust gas enters the FGD unit and is scavenged by precooling and circulating water and further passes through de-misters to the opacity measurement instrument. Table 3.1 lists basic information about the test stack at the power plant. The sampling sites were located in the vertical stack 50 m above the ground. The optical cross-stack transmissometer monitor was located 1.2 m below the sampling ports.

3.2 Opacity measurement instrument

Figure 3.2 illustrates the schematic diagram of the continuous emission monitoring system (CEMS), the opacity instrument. The green LED (with a wavelength of 550 nm) illuminates the projection aperture, and light energy passes through the aperture to the surface mirror. The surface mirror reflects the energy to the beam splitter. Half of the energy is reflected and passes through the stack to the retro reflector for measurements of in-stack flue gas opacity. The energy reflected by the retro reflector passes along the same path through the stack, and further through the beam splitter and field lens aperture to the signal detector which measures the plume opacity.

3.3 Main factors influencing opacity

The variables affecting the in-stack opacity also divided into the following two groups[30]: the controllable and uncontrollable variables. Controllable variables are those related to equipment operation and design. Uncontrollable variables are the characteristics of combustion, equipment operation, and allowable instrument measurements error. Table 3.2 shows both types of variables.

As far as the controllable variables are concerned, the following statements can be made[31]:

- NO_2 emission: Nitrogen dioxide (NO_2) has absorption bands in the visible light range, and, it would affect the opacity. The effect of NO_2 could be controlled with low NO_x burners (LNB).
- Mass emission of particulate matter: the higher the mass concentration of particulate emissions, the higher the opacity. For small particles (0.5μ m) opacity decreases as the deviation from the mean particle size is increased while for large particles (above 2 μ m) the converse is true.
- SOx emission: The pollutant SOx from coal-fired boiler can affect opacity measurements. Most of sulfuric acid gas emissions are SO_2, which can be converted to SO_3 with oxygen. SO_3 can be subsequently reacted with water moisture in the flue gas and at temperatures below the acid dew point condensed into sulfuric acid mist droplets, which will increase the opacity.
- Water moisture content: The amount of moisture in a plume influences opacity measurement. Temperature and humidity conditions can result in the condensation of some of the water vapor in the flue gas, which will increase the opacity.
- Excess air: The excess air with a forced draft fan and induced draft fan will dilute the concentration of particulate matter and subsequently reduce the

opacity.

- Stack gas temperature: The gas temperature influences the relationship between standard and actual volume. The lower the exhaust gas temperature, the higher the particle concentration and hence the higher opacity.
- Light path: The CEMS described in the previous section includes an adjustable light path and further influences the opacity.

As far as the uncontrollable variables are concerned, the following statements can be made:

- Particle density: the lower the density of the particles emitted at a given boiler loading, the larger the number of particles and hence the higher opacity.
- Refraction index of particle: Typical power plant fly ash particles have an index of refraction of about 1.5. However, considering the different combustion characteristics and ash compositions, a range of 1.4 to 1.6 might be expected.
- Color of the plume: The color of the plume is related to the type of fuel burned and the resulting constituents of the particulate matter and flue gas in the plume.

3.4 Experimental method and procedure

To evaluate the effects of various constituents on in-stack opacity, particle mass concentration, water moisture concentration, gaseous oxides of sulfur (SO_x), nitrogen (NO_x), and oxygen (O_2) concentrations, flow rate, flue gas temperature, the circulating water pH of FGD, H_2SO_4, and opacity were measured simultaneously for each run. In order to investigate the formation of in-stack opacity, we change the controllable

variables by adjusting the ESP currents, the FGD unit operating conditions, and boiler loads (BO), respectively. The parenthesis behind each controllable variable in Table 3.2 includes the adjustments that will influence this controllable variable. Two of the controllable variables, the light path and excess air, are kept constant in present study. The ESP currents were regulated to produce various particle concentrations, the precooling and circulating water in the FGD unit were adjusted to produce various mass concentrations of water moisture in the flue gas, and the boiler loads were adjusted by changing the input rate of the coal feeder. When the effect of a load was to be analyzed, the other two loads were set to a relatively steady state to systematically and quantitatively examine its effect on opacity. Note that the operation conditions were limited to those that could not exceed the Republic of China Environment Protection Administration (ROC EPA) emission standards. The in-stack opacity, water moisture, and particle mass concentration were measured simultaneously under various conditions of the boiler load, FGD, and ESP to evaluate their effects on K_p and K_w. The in-stack instruments include an opacity meter, a CEMS, a thermometer, a flow rate meter, and a pH meter. Opacity was measured by an optical transmissometer using a green light-emitting diode with a wavelength of 550 nm. The readings of opacity were recorded every 6 sec. The value of opacity presented in the following is the average of readings at three 6-min intervals. The CEMS is a lineup of analyzers for the measurement of NO_x, SO_x, and O_2 stack gases emitted from the boilers of a thermoelectric coal-fired power plant. The units are capable of the simultaneous and continuous measurement of various components. The temperature of the flue gas was monitored every minute by a resistance thermometer (RTD, type Pt 100). The flow rate of the flue gas was monitored every minute by a supersonic flow rate meter. Table 3.3 showed the accurate analysis of CEMS instruments lists.

3.5 Flue gas sampling methods and analyses

The flue gas was sampled to obtain the mass concentration of particles W_p (mg/Nm^3), the mass concentration of water moisture W_w (g/Nm^3), and the particle size distribution. In addition to the above factors, particle density, particle chemical compositions, and particle shape were also measured. The isokinetic sampling of the ROC EPA Method 1, a modified method of the U.S. Environmental Protection Agency Method 5 with fiberglass thimbles replacing the fiberglass filter, was used to measure the particle mass concentration. The mass concentration of particles was determined by gravimetric analysis of the samples. The water moisture in the stack flue gas was absorbed by calcium chloride ($CaCl_2$) pellets, and the water mass concentration was determined by gravimetric analysis. Sampling of the particles by filter method continued for 30 min, and the total sampled flue-gas volume exceeded 500 L. Sampling of the water content took 10 min, and the total sampled flue-gas flow exceeded 10 L for each sample. The particle size distribution was determined using a cascade impactor with nine impactor stages with cut sizes from 0.1 to 10 μ m, associated with the gravimetric analysis of the samples. To measure the concentration of H_2SO_4, a sample was obtained from the stack gas through a heated quartz-lined probe. The concentration of H_2SO_4 was determined using a method similar to that utilized in Ref. 17, and analysis was conducted on an ion chromatograph. The particle density was analyzed using an ultrapycnometer and by applying Archimedes' principle of fluid displacement and Boyle's law. Particle chemical compositions were analyzed using inductively coupled plasma with atomic emission spectroscopy and by performing standard industrial analyses. The particle shapes were determined using a scanning electron microscope (SEM) from the filter tube. All indicated data are

averages of at least three repeated runs and include the standard deviation. The SOx concentration of the flue gas was controlled using an aqueous magnesium oxide (MgO) solution. The flue gas had passed through the de-mister with an outlet temperature of nearly 50°C. In the FGD unit, the efficiency of SO_x removal test data was up to approximately 99%. The experimental measurements show that when the SO_x concentration increased from 21 to 143 ppm, the concentration of H_2SO_4 increased from 3.1 to 7.7 mg/Nm^3 and the in-stack opacity increased from 24.6 to 25.2%. Because the variation in opacity with a considerable change in SO_x concentration was less than 0.6% and all experiments in this study were performed at a SO_x concentration controlled to within approximately 20–36 ppm, the effects of SO_x and H_2SO_4 emissions on opacity were thus negligible.

Table 3.1 Basic information on the power plant

Parameter	Basic information
Analysis of coal:	
Coal type	Sub-bituminous
Total moisture (as received)	8.89%
Inherent moisture (air-dried basis)	2.01%
Sulfur content (air-dried basis)	0.88%
Volatile matter (air-dried basis)	31.30%
Ash (air-dried basis)	15.20%
Heating value (air-dried basis)	1570 kJ/kg
Boiler conditions:	
Boiler type	four radiative burner units
Coal flow	~1.45-1.72 kg/s
Main steam pressure	~119-120 kg/cm^2
Main steam flow	~ 11.8-13.4 kg/s
Air pollution control equipment	
	1. Low-NOx burner (LNB)
	2. Electrostatic precipitator (ESP)
	3. Flue gas desulfurization (FGD)
Stack parameters:	
Stack height	70 m
Stack diameter	2.4 m

Table 3.2 Summary of the influencing in-stack opacity

Controllable factors－boiler combustion、equipments and design variables:
NO_2 emission (Boiler load)
Mass emission of particulate matter (ESP, Boiler load, FGD)
SO_x emissions with the (FGD, Boiler load)
Water moisture content leaving from (FGD)
Excess air
Stack gas temperature (Boiler load)
Light path
Uncontrollable factors－boiler combustion and measurement
Particle density
Particle index of refraction
Color of the plume

Table 3.3 Schematic the CEMS instruments

Exhaust gas analyzer (measured components: NO_x, SO_2, CO, CO_2 and O_2)
Repeatability:
Ranges≧200 ppm: ± 0.5% of full scale
Ranges≦200 ppm: ± 1.0% of full scale
Zero drift:
Ranges > 200 ppm: ±1.0% of full scale / 7 days
Ranges < 200 ppm: ±2.0% of full scale / 7 days
Span drift:
Linearity: ±1.0% of full scale
Interference: <±2.0% of full scale for standard sample gas composition
Flow
Resolution: 0.03 m/sec
Long-term repeatability: ±0.1m/sec
Relative accuracy: Typically <5% above 3.0/m/sec
Drift: ±1.0%reading over full range
Opacity
Calibration error: 2.0% opacity maximum
Long-term drift
Zero drift: 0.5% opacity maximum
Span drift: 0.5% opacity maximum
Stability over operating temperature range: ±2.0 opacity maximum
Stability over operating main voltage range: ±1.0 opacity maximum

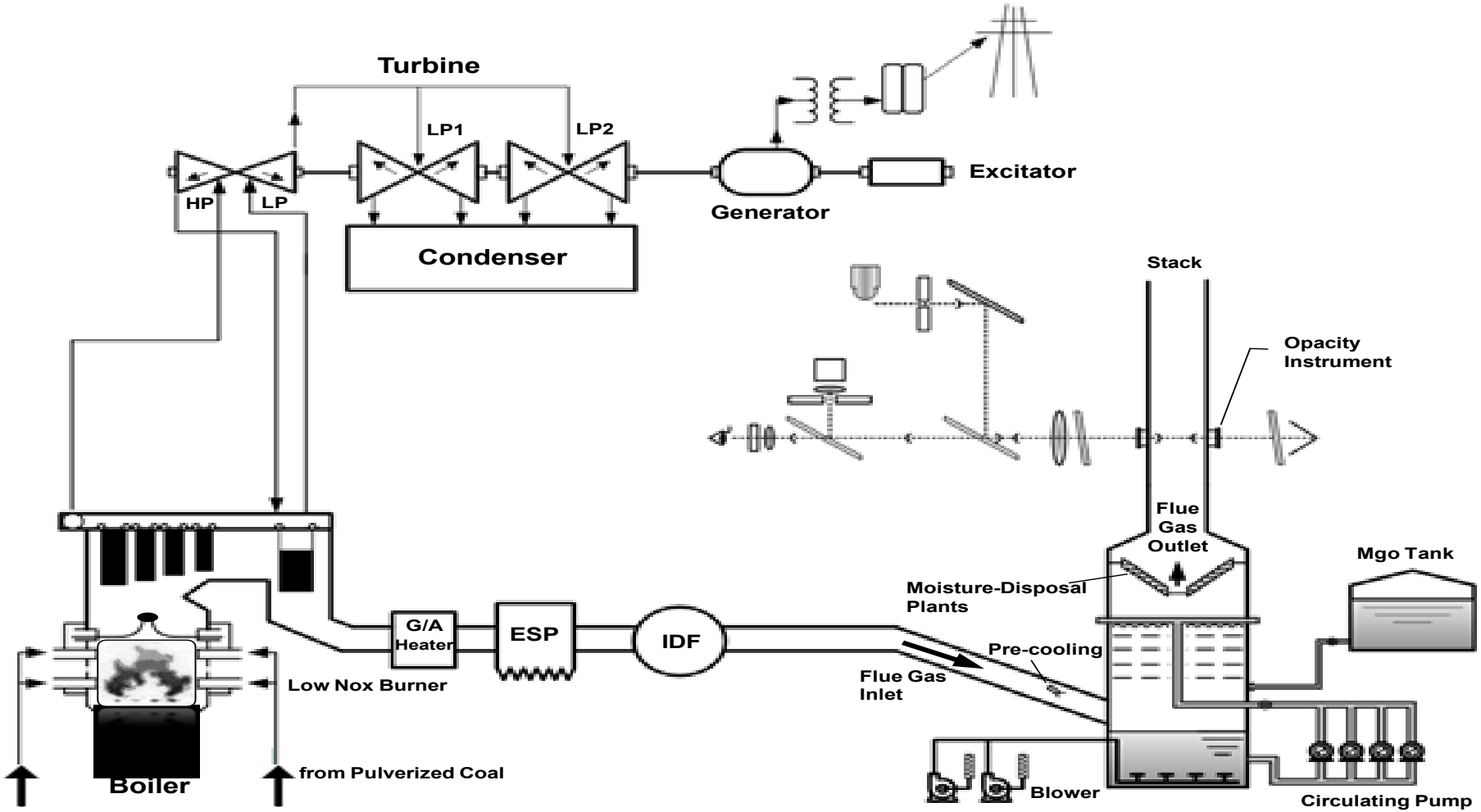

Figure 3.1 Schematic diagram of the coal-fired power plant used in experiments

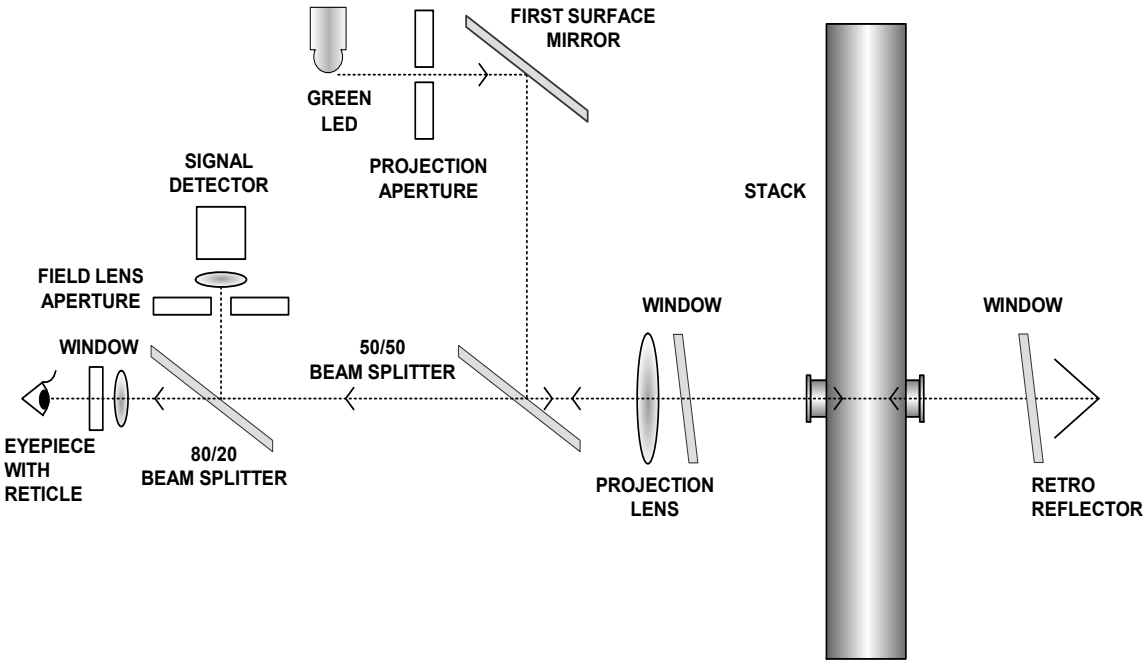

Figure 3.2 Schematic diagram of the optical block diagram.

Chapter 4 Methodology for Estimating Parameters

4.1 Nonlinear least squared method

The parameters W_p, W_w, W_{NO_2}, ρ_p, ρ_w, and ρ_{NO2} in Eq. (2.25) are readily obtained from experimental measurements, while the values of K_p and K_w (or k_p and k_w) remained to be determined. According to Lindau (1991), $1/(K_{NO_2} \times \rho_{NO_2})$ is the mass extinction coefficient k of NO_2 and is measured to be NO_2 concentration (ppm) $\times 3.3\times10^{-4}$ ($ppm^{-1}m^{-1}$). In the present study, the least squares method is used to simultaneously determine the parameters of K_p and K_w measured at various operational conditions. In the present study, the least-square method is used to simultaneously determine the parameters K_p and K_w with measured opacities under various operation conditions.

In the inversion procedure, the squared error, E, is defined as:

$$E = \sum_{i=1}^{n}[Op_{i,c}(K_p, K_w) - Op_{i,e}(K_p, K_w)]^2 = [Y - \eta(\beta)]^T[Y - \eta(\beta)] \quad (4.1)$$

where $Op_{i,e}$ and $Op_{i,c}$ denote the measured and estimated opacities, respectively.

$$Y(i) = \begin{bmatrix} Op_{1,e} \\ \vdots \end{bmatrix}, \quad (4.2)$$

And $\beta = K_p, K_w$. The values of K_p and K_w are determined by minimizing E. The partial derivation of E with respect to β is expressed as:

$$\nabla_\beta E = 2[-\nabla_\beta \eta(\beta)]^T[Y - \eta(\beta)] \quad (4.3)$$

Let $X(\beta) = [\nabla_\beta \eta(\beta)]^T$ (4.4)

where X is the sensitivity matrix, and the elements of this matrix are called the "sensitivity coefficients".[32] When $\nabla E = 0$, the minimum value of E exists, and the

corresponding set of solutions, $\hat{\beta}$, is given by

$$X^T(\hat{\beta})[Y-\eta(\hat{\beta})]=0 \tag{4.5}$$

The Taylor series expansion of $\eta(\hat{\beta})$ at b is

$$\eta(\hat{\beta})=\eta(b)-\nabla\eta(b)(\hat{\beta}-b) \tag{4.6}$$

Substituting Eq. (4.6) into Eq. (4.5) yields:

$$X^T(b)[Y-\eta(b)-X(b)(\hat{\beta}-b)]\approx 0 \tag{4.7}$$

Eq. (4.7) is applied for the numerical computation of the inverse estimation of parameters. Newton's iteration method is used with initial guesses of b. After iterating k times, the $(k+1)$th iteration is started with new parameters:

$$b^{(k+1)}=b^{(k)}+P^{(k)}[X^{T(k)}(Y-\eta^{(k)})] \tag{4.8}$$

and

$$[P^{(k)}]^{-1}=X^{T(k)}X^{(k)} \tag{4.9}$$

The computation continues until the values of K_p and K_w at 2 consecutive calculations differ by a specified limit.

4.2 Sensitivity analysis of parameters

Sensitivity coefficients are very important because they indicate the magnitude of change of the response due to perturbations in the values of the parameters. They appear in relations to many facets of parameter estimation. It is urged to pay particular attention to them and even to plot them versus their independent variables if their shapes are not obvious[33]. In this study, sensitivity coefficient is defined as the derivative of opacity with respect to the parameter, K_p, K_w, W_p and W_w. It describes the quantitative effect of the independent variables on opacity. Sensitivity analyses of the

parameters of W_p, W_w, K_p, and K_w with opacity used data of typical variations in W_p and W_w to give the levels of variation of K_p and K_w. For expression of opacity in Eq. (2.31), the following equations strictly describe the effects of the parameter sensitivity analysis:

$$\frac{\partial Op}{\partial K_p} = \frac{-W_p L}{K_p{}^2 \rho_p} e^{-(\frac{W_p}{K_p\rho_p}+\frac{W_w}{K_w\rho_w}+0.0003W_{NO_2})L} \tag{4.10}$$

$$\frac{\partial Op}{\partial K_w} = \frac{-W_w L}{K_w{}^2 \rho_w} e^{-(\frac{W_p}{K_p\rho_p}+\frac{W_w}{K_w\rho_w}+0.0003W_{NO_2})L} \tag{4.11}$$

$$\frac{\partial Op}{\partial W_p} = \frac{L}{K_p\rho_p} e^{-(\frac{W_p}{K_p\rho_p}+\frac{W_w}{K_w\rho_w}+0.0003W_{NO_2})L} \tag{4.12}$$

$$\frac{\partial Op}{\partial W_w} = \frac{L}{K_w} e^{-(\frac{W_p}{K_p\rho_p}+\frac{W_w}{K_w\rho_w}+0.0003W_{NO_2})L} \tag{4.13}$$

4.3 Theoretical calculation of the particle parameter K_p

Given the wavelength of incident light, particle size distribution, and the complex refractive index of particles, Mie theory can be applied to estimate the particle light extinction efficiency factor, Q_{ext}, which is defined as the ratio of the extinction coefficient to the cross-sectional area for spherical particles. Light extinction by non-spherical particles in random motion was also reported by Hodkinson[34] to be nearly the same as that for spherical particles much larger and much smaller than the wavelength of incident light. In the present study, Q_{ext} is determined using the BHMIE program under equivalent spheres model.

The theoretical parameter, K_p, can then be calculated from Mie theory using:

$$K_p = \frac{\frac{4}{3}\int_{r_1}^{r_2} r^3 f(r)dr}{\int_{r_1}^{r_2} Q_{ext} r^2 f(r)dr} \tag{4.14}$$

where *f(r)* is the normalized particle number density, r is the radius of particles, and Q_{ext} is the particle light extinction efficiency factor.

4.4 Estimation of moisture droplet mean diameter

Moisture molecules may concentrate at flow gas temperature drops, they combine to form water droplets. For a monodispersion of spherical moisture droplets, the relationship between the mass extinction coefficient and extinction efficiency factor can be deduced from Eq.(2.3) and is expressed as:

$$k_w \ W_w = \mathrm{N} Q_{wext} \pi r^2 \tag{4.15}$$

where Q_{wext} is the extinction efficiency factor of a moisture droplet determined by Mie theory, and r is the radius of the moisture droplet. N is the number of moisture droplets per unit volume, and is given from mass concentration of water moisture as $W_w/(4\pi r^3 \rho_w/3)$. The amount of water moisture present in gas can also be described by the expression of relative humidity.

For water moisture, it scatters and does not absorb the beam at the investigated wavelength. And the index of refraction is about 1.33. In the Rayleigh scattering regime, the extinction efficiency factor can be further expressed[35] as:

$$Q_{wext} = \frac{8}{3}\left|\frac{m^2-1}{m^2+2}\right|^2 \left(\frac{2\pi r}{\lambda}\right)^4 \tag{4.16}$$

From Eqs. (2.3), the effective mean diameter (2r) of water moisture droplets can be estimated after the mass extinction coefficient k_w is readily determined.

Chapter 5 Results and Discussion

5.1 Summary of flue gas and characteristics of particles

When pulverized coal is burned in a boiler, most of the ash leaves the furnace (as fly ash) with the flue gas. Table 5.1 shows the composition of flue gas and the constituents of ash under various operation conditions of the boiler load. In this investigation, major compositions of the fly ash particles were SiO_2 (46.9%±0.5%) and Al_2O_3 (42.7%±0.3%); the particles contained 5.8% ~ 7.8% unburned carbon by weight. The particle density is 2.66 ± 0.09 g/cm^3; this density is assumed to be constant over the range of particle sizes measured and is close to the typical soil density. Fig. 5.1 shows the particle size distributions for particle concentrations at various boiler loads. Set #1, #2, and #3 are for particle concentrations of 36.5, 45.6, and 51.5 mg/Nm^3 respectively. Typical mass and cumulative distributions of emitted particles on weight basis are shown in lognormal coordinates, and all of three samples have been equipped with the ESPs. Most of the particles had diameters greater than 0.5 μm, the particle sizes larger than 11μm were 10.5%, and the mass mean diameter was 4.00±1.03 μm. Furthermore, the size particles remained steady with different boiler loads, because the samplings of flue gas were made downstream of the ESPs. The SEM micrographs of particles were presented in Fig. 5.2 and Fig. 5.3. The results from SEM showed that most of particles less than 5 μm were nearly spherical. Cho *et al.*[36] concluded that fine fly ash particles (< 200 mesh) were spherical, while the coarse particles (> 200 mesh) were mostly irregular and porous, which is consistent with the conclusions of Refs. 17 and 18 mentioned earlier.

5.2 Experimental data obtained under various operation conditions

Table 5.2, Table 5.3 and Table 5.4 presents detailed experimental results for variations of ESPs, FGD, and boiler load, respectively, where the various operation conditions were set by regulating ESP currents, adjusting the pre-cooling and circulating water in the FGD unit, and adjusting the main steam flow rate by changing the feeding rate of coal into the boiler. The baseline condition was set as an ESP current of 200mA, the FGD unit pre-cooling and circulating water at 0.36 m^3/s, and the main steam flow rate in the boiler of 12.5 kg/s. From Table 5.2, the opacity increased with decreasing ESP current supply. This relationship follows from the fact that increasing the ESP electric current gradually reduced the particle concentration, as revealed by the measured data. From Table 5.3, which shows the effects of the operation parameters of the FGD unit, the opacity remained almost constant as the operation of the pre-cooling and circulating water varied, because particle mass concentration decreases when water moisture increases and vice versa. From Table 5.4, as the coal flow rate increased with the boiler load, the opacity increased because the mass concentration of the participating constituents and particularly that of the particles increased.

5.3 Influence of particle and water moisture emission on opacity

5.3.1 Inversion estimations of parameters K_p, K_w, k_p and k_w

The values of parameters K_p and K_w were determined from the experimental data in Table 5.2, Table 5.3 and Table 5.4, using the inversion methodology described above. The results show that the values of K_p and K_w were 1.642 cm^3/m^2 and 2520 cm^3/m^2, respectively, corresponding to k_p and k_w values of 0.229 m^2/g and 0.000397 m^2/g, respectively. Although K_p and K_w differ by three orders of magnitude, the effect of extinction by water moisture is comparable to that by particles or even greater due

to the existence of a considerable mass of water moisture after the FGD unit. As illustrated in Table 5.2, Table 5.3 and Table 5.4, which shows that the NO_2 concentration under typical conditions of a coal-fired boiler was in the 4.7-5.7 ppm range with a stack diameter of 2.4 m, NO_2 was responsible for less than 0.90% of opacity. Table 5.5 presents the estimates of parameters K_p and K_w at various loads. For the inversion estimates, the data at various ESP loads produced K_p = 1.522 cm^3/m^2 and K_w = 2596 cm^3/m^2, the data at various FGD loads produced K_p = 1.890 cm^3/m^2 and K_w = 2347 cm^3/m^2, and the data at various boiler loads produced K_p = 1.191 cm^3/m^2 and K_w = 2896 cm^3/m^2. As the mean inversion estimations of a K_w of 1.642 cm^3/m^2 and a K_p of 2520 cm^3/m^2, obtained using all measurements at various loads, are applied to predict the opacity, the numerical results reveal that the measured opacity data are linearly correlated with the values predicted by Lambert-Beer's law, and the regression is 92.94% of confidence.

The experimental uncertainty analysis of parameter K_p and K_w are based on the uncertainties in the experimentally measured quantities that are used in form of mathematical relationship to calculate that derived quantity. The model used to convert the measurements into the derived quantity is usually based on fundamental principles of a science or engineering discipline. Table 5.5 also shows that the mean uncertainty of parameter δ_{kp} and δ_{kw} were 0.00619 cm^3/m^2 and 1.172 cm^3/m^2, respectively.

5.3.2 Theoretical values of particle parameter K_p

The theoretical particle parameter K_p, computed using Eq. (4.14), is determined from the particle number density and the complex refractive index at a given wavelength. The complex refractive index of particles could not be measured directly,

and investigations were based on the experimental measurements of transmittance and/or reflectance as well as a corresponding inverse model such as the equivalent spheres model associated with Lorenz-Mie theory or Rayleigh scattering approximation. The optical properties of fly ashes have been studied by various researchers[20, 37–40]. The real part of the refractive index has been measured in the visible spectral region and was found to vary approximately between 1.5 and 1.6, consistent with results for aluminosilicate glasses in the visible wavelength range. The reported values[39] for the imaginary part of the refractive index, ranging up to approximately 0.05, show considerable variations and may vary by more than an order of magnitude for fly ash samples taken from different power plants. Because the real part of the optical constant is similar to that of its major constituents, an average value of 1.5 may be assigned for fly ashes[39-41], whereas the value of the imaginary part ranges from 0 to 0.024 for fly ashes[41]. The in situ measurements were made by Gupta and Wall[39] at two power stations burning three coals. For these three coals, the values of ash density were found to be 1.78, 1.97, and 2.05 gm/cm^3, respectively. It is shown that the unburned carbon has a substantial effect on the absorption index of fly ash particles, with the carbon-free fly ash being characterized by a lower value of the absorption index. After ashing in a muffle furnace, they recommended the refractive index of 1.5-ni, with n ranging from 0.0035 to 0.025 for fly ashes. In the study presented here, fly ash of complex refractive index 1.5-ni, with n ranging from 0 to 0.05 at light wavelength of 550 nm, was used with the BHMIE program. Three samples of particulate matter are considered, and the detailed distributions of particle size and number density are shown over eight size intervals in Table 5.6. Mean particle size in each interval i was computed, and corresponding K_{pi} values were calculated at an n of 0.0043, 0.01, and 0.025 with the BHMIE computer program. The

results show that the mean theoretical particle parameters, K_p, were 1.334, 1.321, and 1.314 cm^3/m^2, respectively, which are smaller than the measured K_p of 1.642 cm^3/m^2. The corresponding mass extinction coefficients are, respectively, 0.282, 0.285, and 0.286 m^2/g, compared with the measured k_p of 0.229 m^2/g. The result at an n value of 0.05 is very close to that at an n value of 0.025. Fig. 5.4 shows the mean value of the theoretical particle parameter K_p over the particle size range of approximately 0.01–100μ m for absorptive components of the refractive index of 0.0, 0.0043, 0.01, 0.025 and 0.05 respectively. To calculated the monodispersive parameter of K as a function of particle radius and refractive index. For smaller particle sizes, both scattering components and absorptive components of the refractive index are very important. It is illustrated that the effect of absorption index becomes insignificant for particles larger than 0.1μ m at a light wavelength of 550 nm. The parameter of K is evaluated incrementally over the size distribution, it may occur as a function of particle size. The discrepancy in experimental and theoretical results of extinction coefficient may be due in part to a deviation of the actual microstructure of the fly ash from the assumed solid spherical structure because fly ash may have formed as spheres that were attached with smaller particles or as hollow spheres that contained solid spheres. The extinction coefficient of hollow spheres is smaller than that of solid spheres; that is, K_p for solid spheres is smaller[42, 43].

5.3.3 Comparison of experimental parameter K_p with published value

In Table 5.7, the measured values of parameters K_p and k_p are compared with previously reported values obtained without considering water-moisture effects. Published values of K_p are lower than 1.642 cm^3/m^2, ranging from 0.60 to 1.20 cm^3/m^2. The value of the extinction coefficient k_p obtained in this study is 0.229 m^2/g;

published values are larger, ranging from 0.33 to 1.70 m^2/g. Discrepancies between the measurements of K_p and k_p obtained here and those made elsewhere are due mainly to the consideration or lack of the effect of water moisture; previously reported measurements do not consider the effect of the extinction by water moisture. It is reasonable that previously reported values of measured k_p are greater than that obtained in this study because they should reflect the effect of extinction by water moisture present in the flue gas. Moreover, the values of particle density listed in the table were all assumed in their calculations, so this might further influence the accuracy of measurements of the parameters k_p and K_p.

5.3.4 Estimation of the moisture droplet mean diameter

The flue gas had passed through the de-mister with an outlet temperature of nearly 50°C, where the water content in the flue gas was measured. The mole fraction of water moisture, X_w, in gas was then calculated. Because the theoretical mole fraction of water vapor within the saturated flue gas is denoted as X_{wt}, the RH is thus determined as the ratio of X_w to X_{wt}. From Table 5.2, Table 5.3 and Table 5.4, all averages of the measured RH values of the flue gas in this study are less than 100%; only in a few experimental cases did the variation of the actual water content reach the saturated water content. Specifically, values of average RH ranged from 69% to 98.7%. For a mass extinction coefficient k_w equal to 0.000397 m^2/g, the effective mean diameter, 2r, of the moisture droplets is determined from Eq. (2.3) to be approximately 13 nm, whereas the mean diameter of a single water molecule is 0.29 nm. A test was performed to clarify the effect of water moisture on particles and specifically the effect of the absorption of water by particulates. Water was infused into various particle samples, which were obtained at various loads, on filter paper in

the ambient environment, and the dissipation of water by spontaneous mass diffusion was measured. It was found that a major loss of water occurred within the first 4 hr; eventually water absorption by the particles was found to be negligible (<5% by weight).

5.4 Results of sensitivity analysis

The particle properties of particle density and NO_2 emission did not strongly vary from the standard deviation, so they were all set to constant values by applying averages of experimental results, the following equation was derived

$$Opacity = 1 - e^{-(\frac{W_p}{2.66K_p} + \frac{W_w}{K_w} + 0.0017) \times 4.8} \tag{5.1}$$

Sensitivity analyses of the parameters of W_p, W_w, K_p, and K_w with opacity used data of typical variations in W_p and W_w to give the levels of variation of K_p and K_w. Using the differential method with Eq. (5.2) to yield the sensitivity analysis of parameters K_p and K_w, the following equations strictly describe the effects of the parameter sensitivity analysis:

$$\frac{\partial Op}{\partial K_p} = \frac{-1.8W_p}{{K_p}^2} e^{-(\frac{1.8W_p}{K_p} + \frac{4.8W_w}{K_w} + 0.008)} \tag{5.2}$$

$$\frac{\partial Op}{\partial K_w} = \frac{-2.4W_w}{{K_w}^2} e^{-(\frac{1.8W_p}{K_p} + \frac{4.8W_w}{K_w} + 0.008)} \tag{5.3}$$

$$\frac{\partial Op}{\partial W_p} = \frac{-1.8}{K_p} e^{-(\frac{1.8W_p}{K_p} + \frac{4.8W_w}{K_w} + 0.008)} \tag{5.4}$$

$$\frac{\partial Op}{\partial W_w} = \frac{-4.8}{K_w} e^{-(\frac{1.8W_p}{K_p} + \frac{4.8W_w}{K_w} + 0.008)} \tag{5.5}$$

In order to analyze the sensitivity of Eq. (5.2) and (5.3), we calibrated the parameters, K_p = 1.64 cm^3/m^2 and K_w = 2520 cm^3/m^2, using the nonlinear least-squares regression of Newton's method. The parameter, K_p, varied with various W_p and W_w data, and different constant values of K_w also appeared with comparison of the parameters K_p = 1.64 cm^3/m^2 in Fig. 5.5 and K_p = 0.82 cm^3/m^2 in Fig.5.6. Different constant values of K_w also showed a comparison with parameter K_w = 2520 cm^3/m^2 in Fig. 5.7 and K_w = 1260 cm^3/m^2 in Fig.5.8.

Results of Fig. 5.5 show that the maximum sensitivity coefficient of $\frac{\partial Op}{\partial K_p}$ occurred at $W_p = \frac{K_p \rho_p}{L} = 0.909\ g/Nm^3$. Figure 5.6 just changed the K_p value from 1.64 to 0.82 cm^3/m^2, and the results show that the maximum sensitivity coefficient of $\frac{\partial Op}{\partial K_p}$ occurred at $W_p = \frac{K_p \rho_p}{L} = 0.455\ g/Nm^3$. It was more strongly variation associated with a smaller particle concentration. Results of Fig. 5.7 show that the maximum sensitivity coefficient of $\frac{\partial Op}{\partial K_w}$ occurred at $W_w = \frac{K_w \rho_w}{L} = 525\ g/Nm^3$, and that the data were linearly correlated with the figure show. Figure 5.8 also just changed the K_w value from 2520 to 1260 cm^3/m^2, and the results show that the maximum sensitivity coefficient of $\frac{\partial Op}{\partial K_w}$ occurred at $W_w = \frac{K_w \rho_w}{L} = 263\ g/Nm^3$. It was more strongly variation associated with smaller water content. From Fig. 5.5, 5.6, 5.7, and 5.8, the data were all linearly correlated with the figure show. The useful inverse estimates of K_p and K_w.

In order to analyze the sensitivity coefficient of particles and water moisture with Eq. 5.4 and 5.5, we calibrated the exact solution of parameters, K_p = 1.64 cm^3/m^2 and

K_w = 2520 cm^3/m^2, which using the nonlinear least-squares regression of Newton's method. The constant parameters of K_p = 1.64 cm^3/m^2 and K_w = 2520 cm^3/m^2 with variation W_p and W_w shows in Fig. 5.9 and Fig. 5.10. Form the Fig. 5.9 and Fig.5.10 we can give the mass concentration of particles and water moisture sensitivity analysis. The optimum sensitivity coefficients for both particle and water moisture content are all approaching to the zero point. The variation in opacity becomes smaller with per unit mass change at larger value of concentration for both particulate emission and water moisture. Because the limitation of particle emissions with EPA rules, and general operation of the FGD unit, we can not operate the maximum sensitivity of particle and water moisture content.

5.5 Influence of sulfuric acid gas emission on opacity

In the general literature, the opacity is determined using Lambert-Beer's law, which depends on detailed information about the optical and physical properties of particulates. In this section, in addition to particles, the effects of NO_2 and water moisture, the sulfuric acid gas emission (SO_x) and O_2 calibration on in-stack opacity were studied because the legislation limiting the particle's maximum mass concentration from industrial stacks. And it is desirable to determine specific relationships between the correlation opacity standard and particulate matter mass emissions.

The sulfur content of coal can affect opacity measurements because the principal source of pollutant SO_x from coal-fired boiler, most sulfuric acid gas emissions of SO_x is SO_2, the SO_2 can be converted to SO_3, which can subsequently react with water moisture in the flue gas. If this occurs in the stack it will be measured as opacity.

As previously discussed, the little variation in opacity with a considerable change

in sulfuric acid gas emission (SO_x) concentration, the experiments were performed at SO_x concentration controlled to within approximately 20–36 ppm and the effects of SO_x emissions on opacity were thus negligible in order to simply the problem. In order to make sure that the effect of sulfuric gas on opacity is negligible, here we perform a quantitative investigation on how the sulfuric acid gas influences the in-stack opacity.

The SO_x of the flue gas is controlled to 20-36 ppm using a PH sensor-controlled M_gO aqueous mixture. The SO_x emissions were presented in experimental results for variations of ESPs (Table 5.2), FGD (Table 5.3), and boiler load (Table 5.4). Similar to Eq. (2.23), a theoretical equation for opacity which includes the effect of sulfuric acid gas can be written as

$$\begin{aligned} Opacity &= 1-e^{-(W_p k_p + W_w k_w + W_{NO2} k_{NO2} + W_{SOx} k_{SOx})L} \\ &= 1-e^{-(\frac{W_p}{K_p \rho_p} + \frac{W_w}{K_w \rho_w} + \frac{W_{NO2}}{K_{NO2} \rho_{NO2}} + \frac{W_{SOx}}{K_{SOx} \rho_{SOx}})L} \end{aligned} \tag{5.6}$$

where W_{sox} denote the mass concentrations of sulfuric acid gas, ρ_{sox} is the densities of sulfuric acid gas. The parameters K_{sox} (cm^3/m^2) and k_{sox} (m^2/g) are ratio of specific SOx volume to mass extinction coefficient and mass extinction of sulfuric acid gas, respectively.

The least-squares method is again used to simultaneously determine the parameters K_p, K_w and K_{sox} with measured opacities under various operation conditions. Table 5.8 showed the values of K_p, K_w and K_{sox} were 1.605，2817 and 6345 cm^3/m^2, respectively, and the corresponding values of k_p， k_w and k_{sox} are 0.226, 0.000355 and 0.0538 m^2/g, respectively.

A comparison between the estimated values of K_p and K_w in Table 5.8 and Table 5.5 is presented here. It is noted that the estimated values of K_p and k_p are almost the

same for both Tables. The values of K_w in Table 5.8 were larger than those of Table 5.5, so that the k_w in Table 5.8 were smaller than those of Table 5.5. However, the differences are very small. These results indicate that the dependence of opacity on SOx emission is only about 2~3%. Besides, the effect of SOx on opacity is implicitly concealed by the effect of water moisture when we neglect SOx in the least-square inverse estimation.

Table 5.1 Summary of flue gas and particle characteristics

Stack flue gas conditions	Test data range
SOx	~20-36 ppm
NOx	~150-186 ppm
NO_2	~4.7-5.7 ppm
O_2 (at sampling hole of stack)	~9.3%-12.1%
(leaving the G/A heater)	~3.5%-3.8%
Flow rate	~20.3-23.8Nm^3/s
Exhaust gas temperature	~48.1-51.1°C
Water content	~9.25%-12.13%
Particle density	2.66±0.09g/cm^3
Mass mean diameter	4.00±1.03μm
Unburned carbon	6.68%±1.10%
Ash analysis of oxides:	
SiO_2	46.89%±0.53%
Al_2O_3	42.71%±0.26%
Fe_2O_3	3.27%±0.34%
CaO	3.33%±0.26%
TiO_2	1.59%±0.02%
SO_3	0.50%±0.03%
K_2O	0.35%±0.00%
Na_2O	0.14%±0.01%
MgO	0.32%±0.03%
Other	0.91%±1.23%

Table 5.2 Data obtained by regulating ESP currents for various particle concentrations

Range	100~200 mA (current)				
Load	−		→		+
Current (mA)	100	125	150	175	200
Particle concentration W_p (mg/Nm^3)	110.0±6	90.8±5.5	79.1±9.0	70.3±8.5	59.2±5.5
Water content W_w (g/N m^3)	90.2±0.5	92.8±1.1	91.7±1.0	91.1±0.7	90.0±1.8
NO_2 emission (ppm)	5.6±0.1	5.1±0.2	5.4±0.2	5.3±0.3	4.7±0.1
SO_x emission (ppm)	25.6±1.2	26.3±0.7	32.4±3.2	35.5±0.5	25.4±0.9
O_2 content (%)	10.6±0.1	10.2±0.1	10.1±0.1	10.6±0.3	11.0±0.1
Flue gas temperature (°C)	50.5±0.4	51.1±0.3	50.3±0.6	49.9±0.4	50.9±0.6
Water content X_w (%)	11.2±0.1	11.6±0.1	11.4±0.1	11.3±0.1	11.2±0.2
Saturated vapor content X_{tw} (%)	12.7±0.1	13.1±0.3	13.0±0.2	12.3±0.3	13.3±0.2
Relative humidity (%)	88.4±0.4	88.1±2.9	88.1±0.5	92.4±2.5	84.3±2.6
Measured opacity (%)	25.7±0.6	24.7±0.4	23.7±0.3	22.7±0.5	20.9±0.6
Theoretical opacity (%)	26.0	24.8	23.7	22.8	21.7
Extinction coefficient by particles eimssion (%)	40.2	35.1	32.2	29.8	26.7
Extinction coefficient by water moisture (%)	56.9	62.1	64.7	66.9	70.2
Extinction coefficient by NO_2 emission (%)	2.9	2.8	3.1	3.3	3.1

Table 5.3 Data obtained by adjusting FGD unit's pre-cooling and circulating water rate

Range	0.27~0.40 m^3/s (circulating water)				
Load	−		→		+
Circulating water (m^3/s)	0.27	0.31	0.33	0.35	0.4
Particle concentration W_p (mg/N m^3)	83.4±8.1	74.2±9.0	70.1±8.9	59.2±5.5	37.8±1.9
Water content W_w (g/N m^3)	74.4±1.8	80.3±1.6	81.5±1.7	90.0±1.8	97.5±0.3
NO_2 emission (ppm)	4.8±0.1	4.6±0.2	5.3±0.1	4.7±0.1	5.1±0.2
SO_x emission (ppm)	25.0±1.8	27.5±2.5	30.8±5.4	25.4±0.9	32.2±1.7
O_2 content (%)	10.3±0.1	10.1±0.4	10.2±0.1	11.0±0.1	11.1±0.1
Flue gas temperature (°C)	50.3±0.5	50.1±0.4	49.1±0.5	50.9±0.6	50.4±0.4
Water content X_w (%)	9.3±0.2	10.0±0.2	10.2±0.2	11.2±0.2	12.1±0.1
Saturated vapor content X_{tw} (%)	13.4±0.2	12.6±0.4	11.9±0.4	13.3±0.2	13.2±0.5
Relative humidity (%)	69.0±2.5	79.6±4.0	85.0±0.7	84.3±2.6	92.3±3.7
Measured opacity (%)	21.5±0.1	21.0±0.4	21.0±0.3	20.9±0.6	21.7±0.7
Theoretical opacity (%)	21.3	21.5	21.4	21.7	21.0
Extinction coefficient by particles emission (%)	38.1	33.8	32.0	26.7	17.7
Extinction coefficient by water moisture (%)	58.8	63.2	64.5	70.2	78.9
Extinction coefficient by NO_2 emission (%)	3.1	3.0	3.5	3.1	3.4

Table 5.4 Data obtained by varying the operation condition of the boiler load

Range	11.78~13.44 kg/s (main steam flow)				
Load	−	→			+
Main steam flow (kg/s)	11.78	12.58	12.89	13.00	13.44
Particle concentration W_p (mg/N m^3)	45.5±1.9	59.2±5.5	66.1±1.9	78.7±2.8	96.6±1.7
Water content W_w (g/N m^3)	87.7±0.6	90.0±1.8	94.8±2.6	91.6±1.5	89.6±0.3
NO_2 emission (ppm)	5.0±0.4	4.7±0.1	5.0±0.4	5.3±0.2	5.7±0.1
SO_x emission (ppm)	24.0±3.9	25.4±0.9	36.0±1.6	33.2±2.4	33.0±1.4
O_2 content (%)	10.8±0.2	11.0±0.1	10.9±0.1	11.0±0.2	10.6±0.2
Flue gas temperature (°C)	48.1±0.4	50.9±0.6	49.3±0.2	50.3±0.6	49.3±0.4
Water content X_w (%)	10.9±0.1	11.2±0.2	11.8±0.3	11.4±0.2	11.2±0.1
Saturated vapor content X_{rw} (%)	11.1±0.1	13.3±0.2	12.0±0.1	11.9±0.5	11.6±0.2
Relative humidity (%)	98.7±1.2	84.3±2.6	98.2±2.6	95.6±4.0	96.1±0.9
Measured opacity (%)	19.8±0.3	20.9±0.6	22.7±0.3	24.6±0.7	25.6±0.3
Theoretical opacity (%)	20.2	21.7	23.0	23.6	24.9
Extinction coefficient by particles emission (%)	22.3	26.7	27.9	32.1	37.2
Extinction coefficient by water moisture (%)	74.2	70.2	69.1	64.8	59.7
Extinction coefficient by NO_2 emission (%)	3.5	3.1	3.0	3.1	3.1

Table 5.5 Results of K_p, K_w, k_p and k_w, estimated from measurements

Parameter	ESP operation	FGD operation	Boiler operation
K_p (cm^3/m^2)	1.522	1.890	1.191
uncertainty,δ_{kp}	0.00762	0.00658	0.00367
Mean K_p (cm^3/m^2)		1.642	
uncertainty,δ_{kp}		0.00619	
k_p (m^2/g)	0.247	0.199	0.316
Mean k_p (m^2/g)		0.229	
K_w (cm^3/m^2)	2596.1	2346.7	2896.0
uncertainty,δ_{kw}	1.003	1.255	1.242
Mean K_w (cm^3/m^2)		2520.2	
uncertainty,δ_{kw}		1.173	
k_w (m^2/g)	0.000385	0.000426	0.000345
Mean k_w (m^2/g)		0.000397	

* ρ_p= 2.66 g/cm^3, ρ_w= 1.00 g/cm^3.

Table 5.6 Calculated values of the theoretical particle parameter K_p for the measured particle size distribution at various absorption indices

Set	Particle Diameter size interval (μm)	Mean Particle radius (μm)	Mass fraction interval (%)	Accum. Weight fraction (%)	K_{pi} *at m=1.5 n=0.0043* (cm^3/m^2)	K_{pi} *at m=1.5 n=0.01* (cm^3/m^2)	K_{pi} *at m=1.5 n=0.025* (cm^3/m^2)
No.1	>9.3	10.00	5.11	100.0	6.536	6.413	6.401
	6.0-9.3	3.825	4.69	94.89	2.322	2.344	2.358
	4.1-6.0	2.525	10.82	90.20	1.496	1.477	1.506
	2.8-4.1	1.725	15.31	79.38	1.162	1.095	1.053
	1.8-2.8	1.150	33.06	64.07	0.737	0.708	0.685
	1.0-1.8	0.700	16.73	31.01	0.527	0.493	0.461
	0.49-1.0	0.373	9.18	14.28	0.115	0.118	0.123
	0.36-0.49	0.213	3.47	5.10	0.119	0.118	0.117
	0.056-0.36	0.104	1.63	1.63	0.410	0.333	0.298
	K_p (cm^3/m^2)				1.284	1.252	1.233
	k_p (m^2/g)				0.293	0.300	0.305
No.2	>11.0	10.00	10.97	100.0	6.441	6.413	6.401
	7.1-11.0	4.525	3.95	89.03	2.901	2.868	2.829
	4.8-7.1	2.975	8.55	85.08	1.862	1.848	1.827
	3.3-4.8	2.025	14.69	76.53	1.102	1.126	1.165
	2.2-3.3	1.375	29.61	61.84	0.808	0.800	0.794
	1.1-2.2	0.825	17.54	32.23	0.456	0.454	0.450
	0.59-1.1	0.423	11.18	14.69	0.149	0.150	0.155
	0.44-0.59	0.258	2.19	3.51	0.102	0.103	0.105
	0.056-0.44	0.124	1.32	1.32	0.252	0.243	0.224
	K_p (cm^3/m^2)				1.624	1.623	1.629
	k_p (m^2/g)				0.231	0.232	0.231
No.3	>9.9	10.00	3.29	99.99	6.447	6.413	6.401
	6.4-9.9	4.075	6.85	96.71	2.568	2.554	2.533
	4.3-6.4	2.675	10.68	89.85	1.559	1.571	1.598
	3.0-4.3	1.825	30.68	79.17	1.172	1.152	1.118
	1.9-3.0	1.225	14.52	48.49	0.810	0.795	0.762
	1.0-1.9	0.725	14.52	33.97	0.486	0.474	0.452
	0.53-1.0	0.383	12.33	19.45	0.119	0.121	0.127
	0.39-0.53	0.230	3.56	7.12	0.107	0.107	0.108
	0.056-0.39	0.112	3.56	3.56	0.304	0.293	0.265
	K_p (cm^3/m^2)				1.095	1.089	1.081
	k_p (m^2/g)				0.343	0.345	0.348
Mean K_p (cm^3/m^2)					1.334	1.321	1.314
Mean k_p ($1/(\rho_p K_p)$, m^2/g)					0.282	0.285	0.286

Table 5.7 Comparison of measured K_p values with previously reported values from experiments on coal-fired boilers

Source	Apparatus	Light path (m)	Parameter k_p (m^2/g)	Density ρ_p (g/cm^3)	Parameter K_p (cm^3/m^2)	Reference (No.)
Coal power plant (fly ash)	Transmissometer	4.80	0.228	2.66	1.642	Present study
Coal power plant (fly ash)	Transmissometer	6.15	1.11~1.56	1.00	0.683~0.905	9
Coal power plant (fly ash)	Bolometer	1.14	0.78	2.00	0.64	8
Kraft mill recovery furnace	Bolometer	1.52	1.70	1.00	0.60	6
Kraft mill recovery furnace	Smoke meter	0.92	0.33~0.50	2.50	0.80~1.20	7

Table 5.8 Results of K_p, K_w, K_{SOx}, k_p, k_w and k_{SOx}, estimated from measurements.

Parameter	ESP operation	FGD operation	Boiler operation
K_p (cm^3/m^2)	1.474	2.002	1.260
Mean K_p (cm^3/m^2)		1.665	
k_p (m^2/g)	0.255	0.188	0.298
Mean k_p (m^2/g)		0.226	
K_w (cm^3/m^2)	3096	2817	3153
Mean K_w (cm^3/m^2)		2817	
k_w (m^2/g)	0.000323	0.000355	0.000317
Mean k_w (m^2/g)		0.000355	
K_s (m^2/g)	6113	4022	9596
Mean K_s (cm^3/m^2)		6345	
k_s (m^2/g)	0.0558	0.0849	0.0355
Mean k_s (m^2/g)		0.0538	

ρ_p= 2.66 g/cm^3, ρ_w= 1.00 g/cm^3, ρ_s= 0.00293 g/cm^3

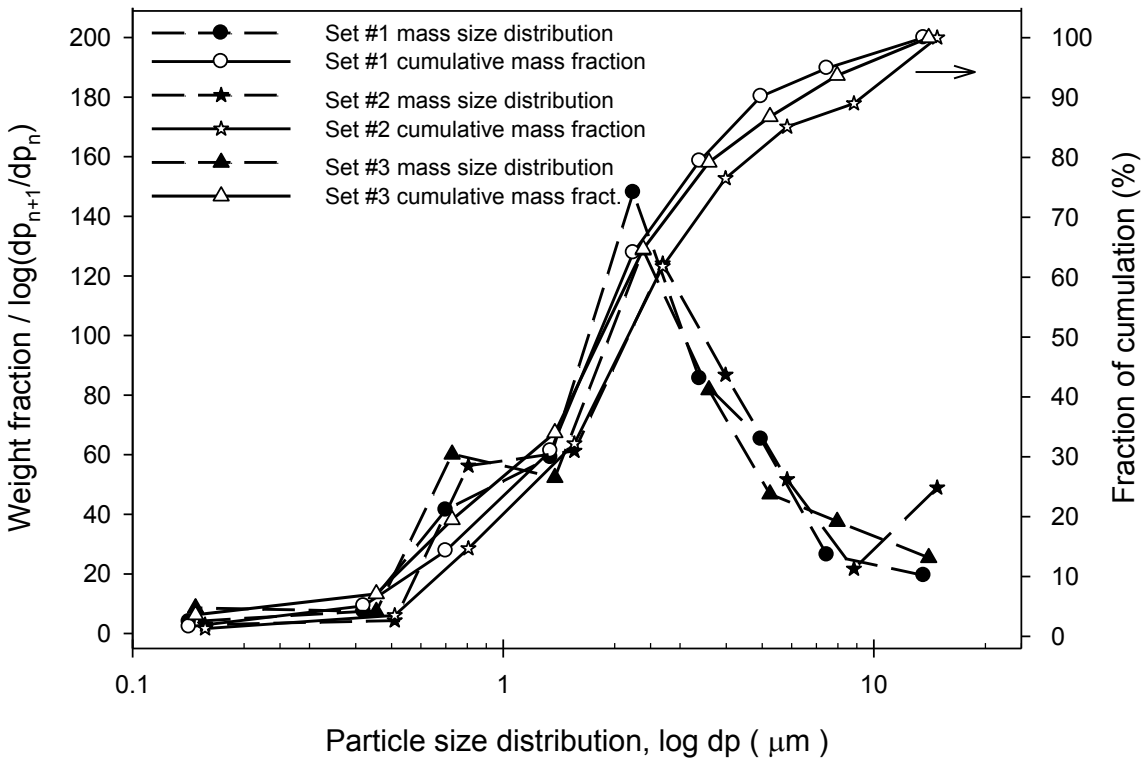

Figure 5.1 Mass and cumulative distributions of emitted particles at various boiler loads (Set #1, #2, and #3 are for particle concentrations of 36.5, 45.6, and 51.5 mg/Nm^3 respectively)

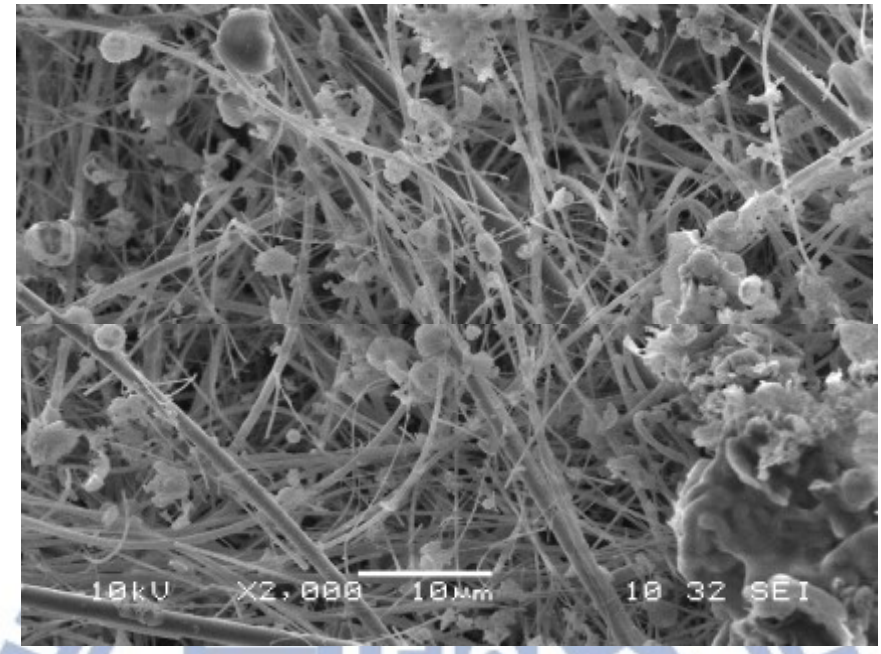

Figure 5.2 SEM micrograph of particles collected by filter

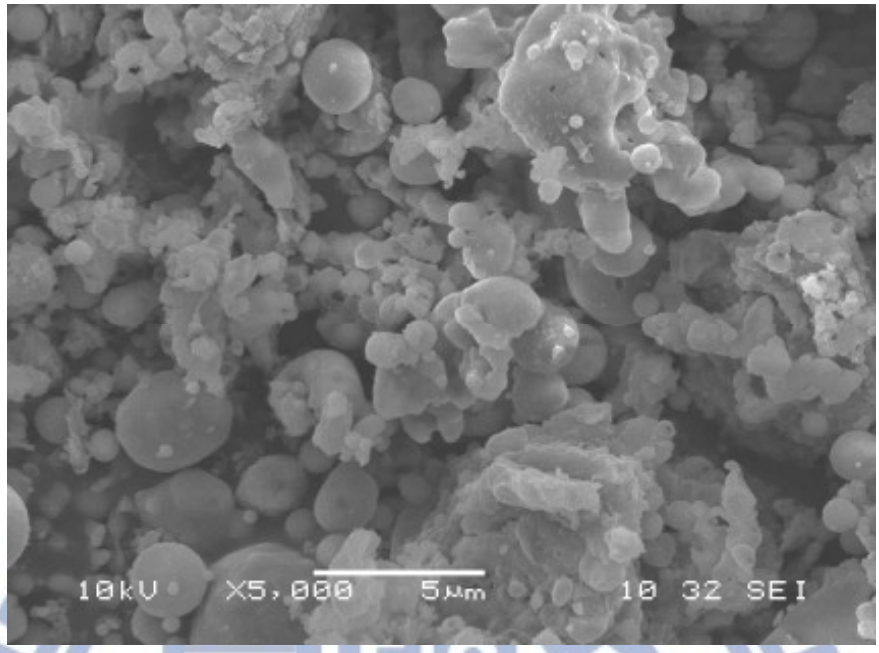

Figure 5.3 SEM micrograph of particles of filter cake

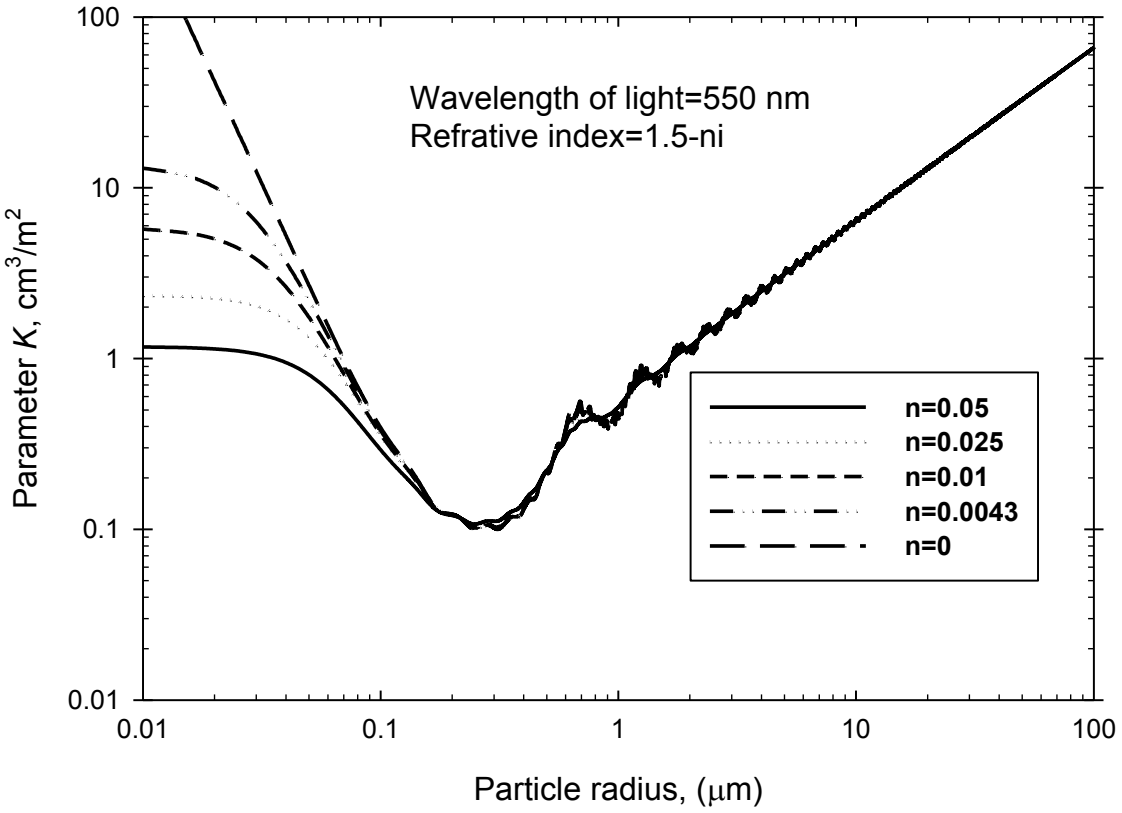

Figure 5.4 Theoretical parameter K_p as a function of particle size for fly ash at various values of absorption index and a light wavelength of 550 nm

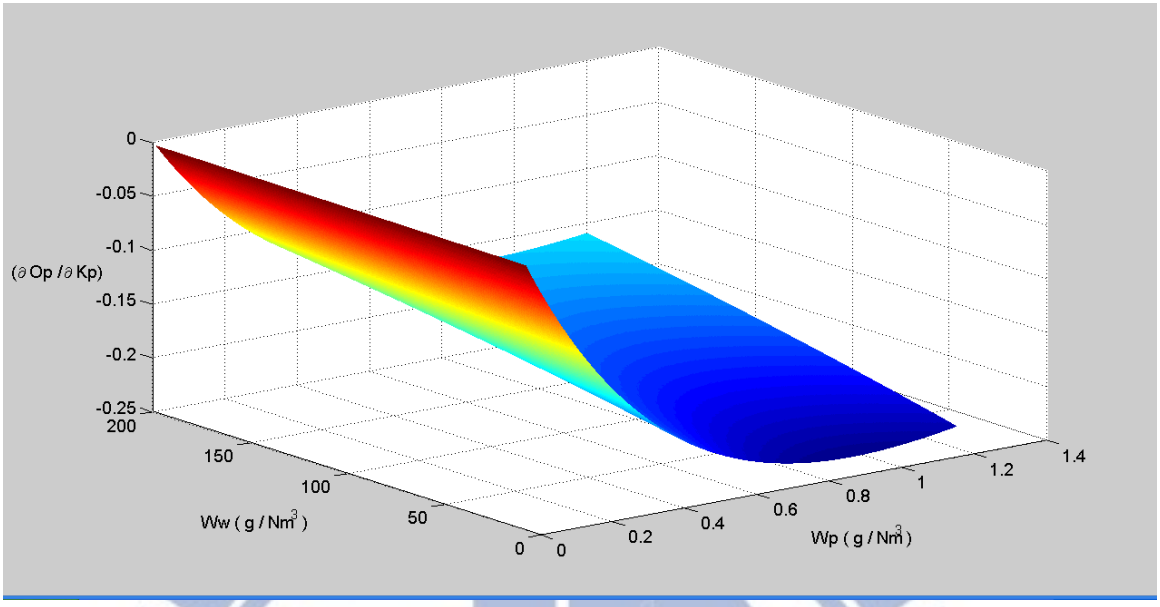

Figure 5.5 Sensitivity coefficient variation $\frac{\partial Op}{\partial K_p}$ at K_P=1.64cm^3/Nm^2, K_w=2520cm^3/Nm^2

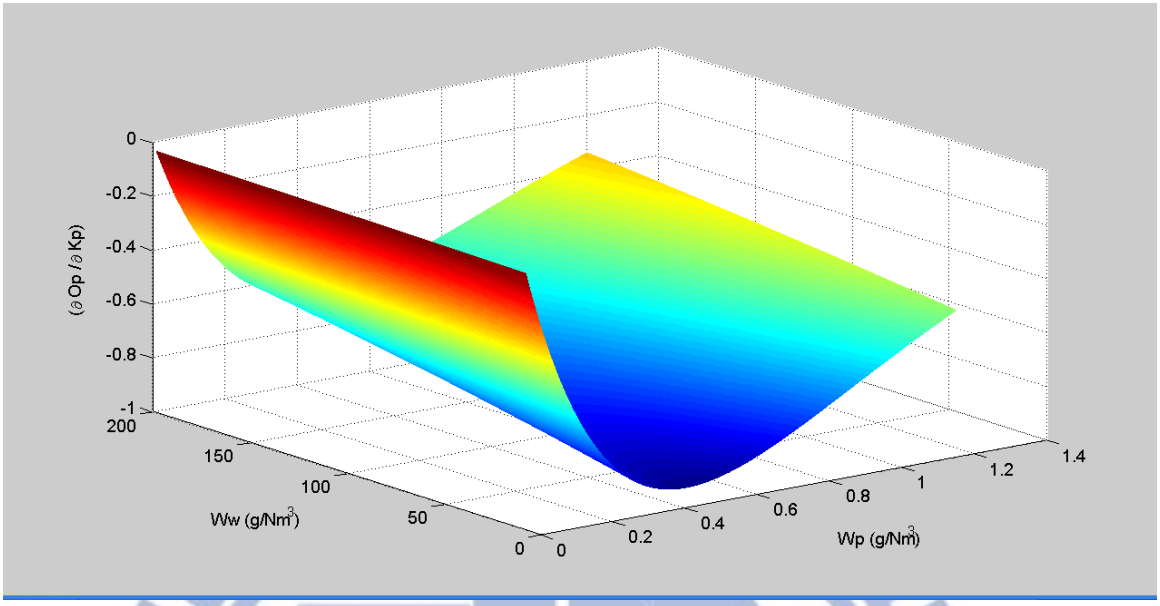

Figure 5.6 Sensitivity coefficient variation $\frac{\partial Op}{\partial K_p}$ at K_P=0.82cm^3/Nm^2, K_w=2520cm^3/Nm^2

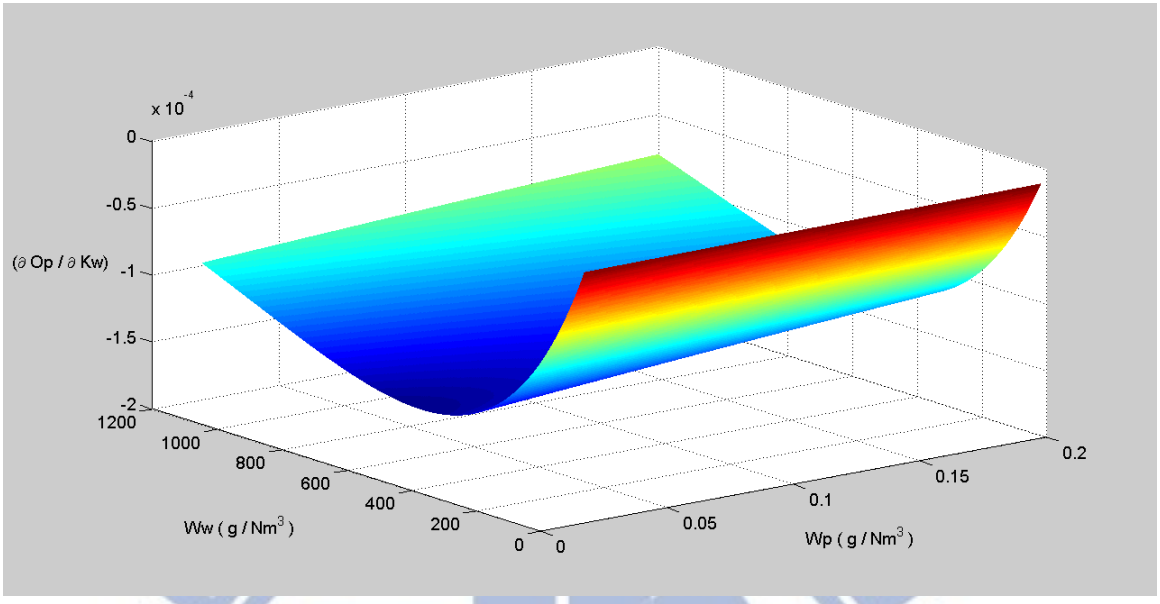

Figure 5.7 Sensitivity coefficient variation $\frac{\partial Op}{\partial K_w}$ at K_P=1.64cm^3/Nm^2, K_w=2520cm^3/Nm^2

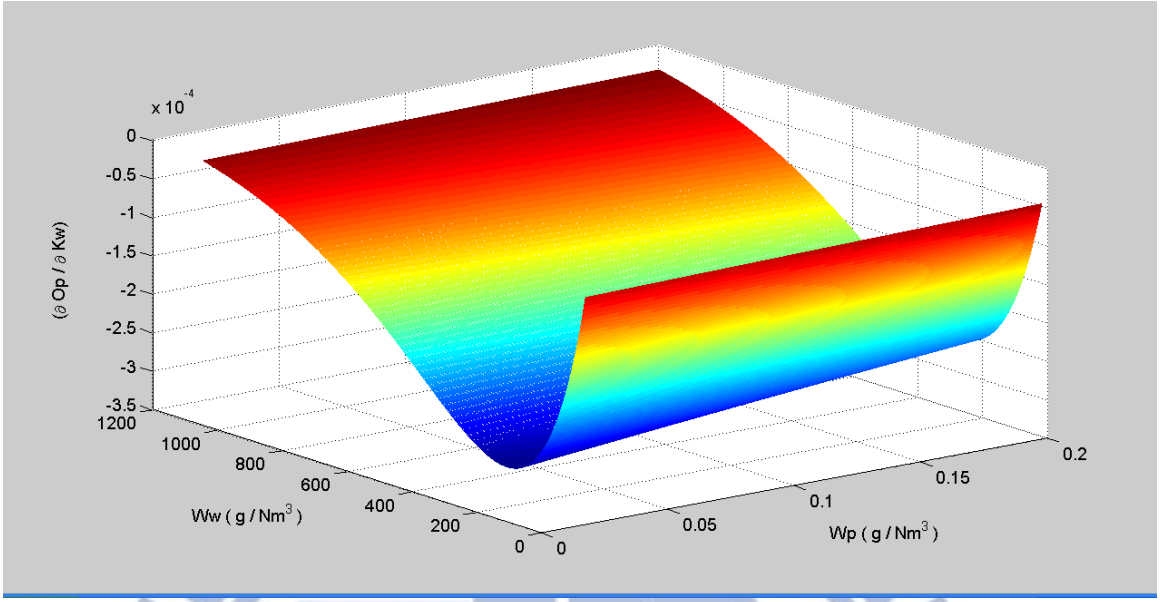

Figure 5.8 Sensitivity coefficient variation $\frac{\partial Op}{\partial K_w}$ at K_P=1.64cm^3/Nm^2, K_w=1260cm^3/Nm^2

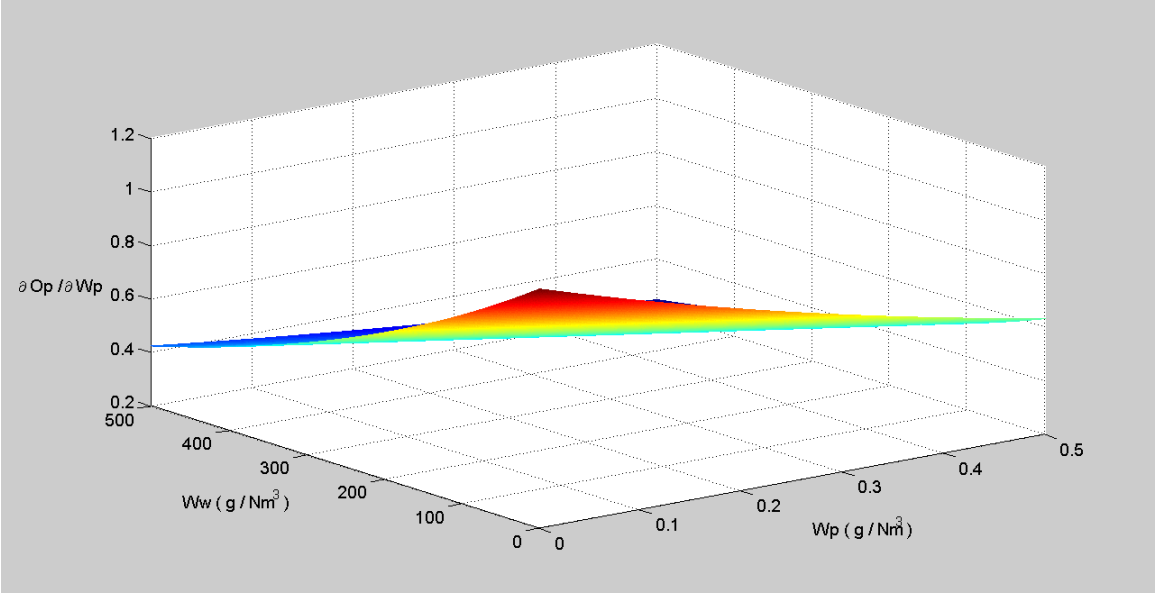

Figure 5.9 Sensitivity coefficient variation $\frac{\partial Op}{\partial W_p}$ at K_P=1.64cm^3/Nm^2, K_w=2520cm^3/Nm^2

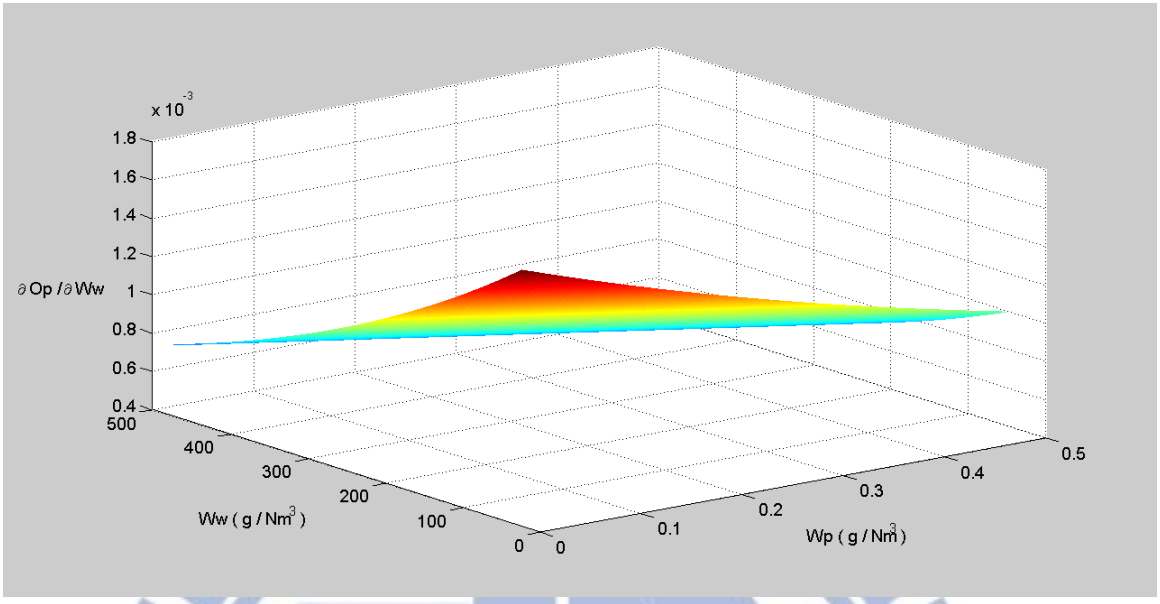

Figure 5.10 Sensitivity coefficient variation $\frac{\partial Op}{\partial W_w}$ at K_P=1.64cm^3/Nm^2, K_w=2520cm^3/Nm^2

Chapter 6 Opacity Correlation Study

This study illustrates the theoretical basis for correlating opacity and particulate mass emission limits at a coal-fired power plant. And it is common for concentration emissions standards to be corrected to a specific oxygen (O_2) concentration. Because the concentration emissions standards are corrected to a specified O_2 concentration, any sources cannot allow more ambient air into the exhaust gas stack. In addition to determining specific relationships between the measured standard opacity and particulate matter mass emissions, the opacity standard was used to establish a range (with 95% confidence interval) of particulate matter concentrations with the appropriate t-statistic.

6.1 Correcting oxygen calibration with particle mass emission[44, 45]

Pollution concentrations are adjusted to the O_2 concentration specified in a standard according to the following equation:

$$Conc.i_{(Std.O_2)} = Conc.i_{(Measured\ O_2)}\left(\frac{21\% - Std.O_2\%}{21\% - Measured\ O_2\%}\right) \quad (6.1)$$

where Conc. $i_{(Std.\ O2)}$ is the pollutant concentration at the O_2 level specified in the standard. Conc. $i_{(Measured\ O2)}$ is the pollutant concentration measured in the exhaust stack. 21% is O_2 concentration in the atmosphere. Std. O_2% is O_2 concentration specified in the standard.

Particulate mass emission limits were calculated based on the Environmental Protection Administration (EPA) rules of Taiwan and the following equation was used to convert W_p to the units of mg/Nm^3 at 6% O_2.

$$W_p' = W_p \times \frac{21\% - O_2\%}{21\% - 6\%} \quad (6.2)$$

where W_p is particle mass concentration, mg/Nm^3, dry basis 21% is O_2 concentration in the atmosphere. O_2 is flue gas oxygen content, %. W_p' is particle mass concentration at 6% O_2, mg/Nm^3, on a dry basis.

6.2 Correlation of opacity empirical equation

The expression of opacity in consideration of oxygen, water moisture and NO_2 can be written as

$$Opacity = 1 - e^{-\left(\frac{W_p}{K_p \rho_p} \times \frac{21 - O_2}{21 - 6} + \frac{W_w}{K_w \rho_w} + \frac{W_{NO2}}{K_{NO2} \rho_{NO2}}\right) L} \tag{6.3}$$

The effect of particle concentrations on opacity was evaluated by examining various parameters and the experimental data are given in Table 5.2 to 5.4. In these tables, almost all values of the opacity corresponding to various concentrations of particulate emissions were more than 20%. The main reason was that the wet desulfurization characteristics caused a high concentration of moisture. According to the law of EPA Taiwan, the upper limit on in-stack opacity is 20% for particulate emission in a coal-fired power plant. By neglecting the effect of water moisture and NO_2 (W_w = 0 and NO_2 = 0), this corresponds to a concentration of W_p= 203 mg/Nm^3 (for 6% O_2 calibration). According to Eq. (6.2), we then calibrate the particulate concentration of our experimental data in Table 5.2 to 5.4. It is noted that the maximum particulate emission is only 158.7 mg/Nm^3 (for 6% O_2 calibration), which is much less than the value of W_p= 203 mg/Nm^3 (for 6% O_2 calibration). From our experimental data shown in Tab. 5.2 to 5.4, an average value of oxygen concentration is about 10.7%. Using the average of our experimental data (W_w = 91.1 g/Nm^3, O_2 = 10.7% and NO_2 = 5.2 ppm), from Eq. (6.3), an opacity of 33.8% is deduced. This is much larger than the upper limit of the law of EPA.

6.3 An empirical opacity correlation[44]

It is useful to give an empirical correlation between opacity and the particulate emission. In general, the correlation can be derived by applying statistical technique to determine boundaries around the expected correlation relationship based on the ± 95% confidence intervals:

$$\text{Opacity}(\%) = \text{Op}_{\text{pre}} \pm \text{t} \times \text{Sy} \tag{6.4}$$

where Op_{pre} is the theoretical predicted value of opacity from Eq. (6.3), t is student t-distribution and Sy is the standard error.

The number of degrees of freedom is the number of samples minus one, and the value of the variance is constant around the predicted value. The standard error of the estimate is calculated as the square root of the sum of the squares of the residuals divided by the number of degrees of freedom as following equation:

$$s_y = \sqrt{\frac{\sum(residuals)^2}{degrees\ of\ \ freedom}} = \sqrt{\frac{\sum(Op - Op_{est})^2}{a-1}} \tag{6.5}$$

where *a* is experimental samples. When this value is multiplied by the appropriate Student's *t*-statistic, it establishes a range around the estimate that establishes the 95% confidence interval for any predicted value.

Since the normal distributions of effective samples are usually located within the 95% interval, the general area of the 95% confidence intervals were approved as standards. The averages of experimental data in Tab. 5.2 and Tab. 5.4 are W_w = 91.1 g/Nm^3, O_2 = 10.7% and NO_2 = 5.2 ppm. Details of the calculation of confidence intervals are shown in Tab. 6.1. The standard error and the appropriate Student's t are calculated to be S_y = 0.61 and t = 2.26, respectively. And the confidence interval is ± 1.38. The concentration of particulate matter and opacity in Eq. (6.4) can be expressed

as:

$$Opacity\ (\%) = 100 - 85.1e^{-0.748W_p} \pm 1.38 \qquad (6.6)$$

Figure 6.1 shows the correlation of Eq. (6.6) and the measured values. It is noted that all measured values are within the range of 95% confidence intervals.

Table 6.1 Estimation of 95% confidence interval boundaries for opacity

	Op	Op_{est}	$(Op\text{-}Op_{est})^2$	W_p	W_p (6% O_2) correction	Upper 95% interval	Lower 95% interval
	%	%	%	mg/Nm^3	mg/Nm^3	%	%
ESP	25.7	26.0	0.09	110.0	158.7	27.2	24.8
	24.7	24.8	0.01	90.8	126.1	26.0	23.6
	23.7	23.7	0.00	79.1	108.9	24.9	22.5
	22.7	22.8	0.01	70.3	101.4	24.0	21.6
	20.9	21.7	0.64	59.2	88.8	22.9	20.5
Boiler Load	19.8	20.2	0.16	45.5	66.9	21.2	19.0
	20.9	21.7	0.64	59.2	88.8	22.9	20.5
	22.7	23.0	0.09	66.1	98.2	24.2	21.8
	24.6	23.6	1.00	78.7	118.1	24.8	22.4
	25.6	24.9	0.49	96.6	139.3	26.1	23.7

Residual square = $(Op\text{-}Op_{est})^2$ =2.95

Standard error $Sy = [(Op\text{-}Op_{est})^2/(n\text{-}1)]^{1/2} = 0.61$

Appropriate student-t $=2.26_{(0.025,9)}$

Confidence interval = $\pm t \times Sy = 2.26 \times 0.61 = 1.38$

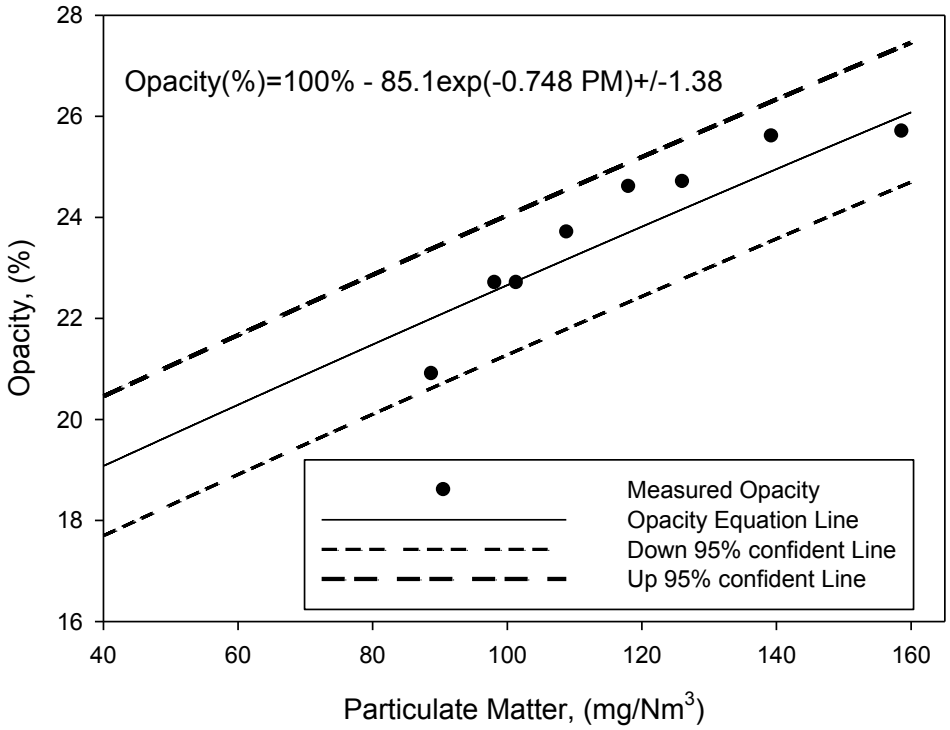

Figure 6.1 Theoretical emissions correlation with ± 95% confidence intervals

Chapter 7 Conclusions and Future works

7.1 Conclusions

Because emission standards have become increasingly strict, FGD with wet scrubbing is generally used for coal-fired power plants. However, after a FGD unit with wet scrubbing is set up, the concentration of water moisture increases, affecting the measured opacity. In this study, the experimental equipments for simulating the formation of opacity under different operational conditions have been designed. With these equipments, the influences of different variables were also studied. Two factors that greatly affect opacity were identified: the mass of emitted particles and the amount of water moisture. The effects of SOx emissions range within 20–36 ppm on the opacity were little variation. The opacity was expressed in the form of the Lambert-Beer law, and a nonlinear least-squares regression was conducted to evaluate the two optical parameters K_p and K_w. The measured K_p of 1.642 cm^3/m^2 is larger than the theoretical values of K_p ranging from 1.314 to 1.334 cm^3/m^2 at various values of absorption index. The effect of absorption index becomes insignificant for particles larger than 0.1μ m. The discrepancy in measured extinction coefficient and theoretical values may be assumed to have a solid spherical structure, whereas the fly ash may have been formed as spheres that were attached with smaller particles or as hollow spheres that contained solid spheres. Moreover, the obtained K_p value of 1.642 cm^3/m^2 is larger than previously reported values of K_p; that is, the corresponding mass extinction coefficient (k_p 0.229 m^2/g) is smaller than previously reported values of k_p. In previous studies, they did not consider water moisture effects and assumed a specific value for the particle density, which might further influence the accuracy of inverse estimations of K_p and k_p.

To determine the quantitative effect of the independent variables on opacity, sensitivity analyses using a correlation equation for opacity with particle emissions as well as concentrations of moisture and nitrogen dioxides were also conducted. Results on sensitivity analyses illustrate that at larger value of the parameter for either particles or water moisture, the influence of the exhaust emission on the opacity becomes smaller. Finally, an empirical correlation between opacity and particulate concentration is given with 95% confidence intervals by taking water moisture, SOx, NOx and oxygen calibration into consideration. Predictions of opacity using light-scattering theory and measurements of the stack gas opacity were in good agreement. Results also indicate that the in-stack opacity could increase to 33.8% but still fulfill the requirement of EPA limit when water moisture is taken into consideration.

7.2 Future works

The present study analyzes the effect of water moisture and sulfuric gas emission on the in-stack opacity of a coal-fired power plant. In order to get more physical insight of formation of in-stack opacity, some future works are illustrated in the following. In this study, due to the limitation of EPA rule on emission, only a small range of sulfuric gas emission is investigated. It is worthwhile to design a Lab experiment to investigate the full range effect of sulfuric oxides on opacity. Besides, as the information about extinction coefficient of sulfuric oxides is still lack in the reference, a measurement of extinction coefficient of sulfuric oxides needs to be investigated. The diameter of water moisture is assumed uniform in present study. The effect of size dispersion of water moisture on in-stack opacity measurement should be examined in order to get more accurate opacity correlations. Although the absorption

band of water is fully understood, the size dispersion of water droplet in different thermodynamic states is still a key issue to be explored.

References

1. Watson, J. G. Visibility: Science and Regulation. *J. Air & Waste Manage. Assoc.* **2002**, 52, 628-713.
2. Toro, R. F. *Source Control-food*. Handbook of Air Pollution Technology; Edited by Calvert S.; Englund H. M.; John Wiley & Sons: New York, **1984**; p 376.
3. Lindau, L. NO_2 Effect on Flue Gas Opacity. *J. Air & Waste Manage. Assoc*. **1991**, 41, 1098.
4. Mulholland, G. W.; Choi, M. Y. Measurement of the Mass Specific Extinction Coefficient for Acetylene and Ethane Smoke Using the Large Agglomerate Optics Facility. *Twenty-Seventh Symposium (International) on Combustion*；The Combustion Institute：Pittsburgh, **1998**；pp 1515-1522.
5. Bosch, J. C. Size Distributions of Aerosols Emitted from a Kraft Mill Recovery Furnace. M.S. Thesis, Chem. Eng. University of Washington, DC, **1969**.
6. Larssen, S.; Ensor, D. S.; Pilat M. J. Relationship of Plume Opacity to the Properties of Particulates Emitted from Kraft Recovery Furnaces. *Tech. Assoc. the Pulp and Paper Ind. (TAPPI).* **1972**, 55, 88-92.
7. Thielke, J. F.; Pilat, M. J. Plume Opacity Related to Particle Mass Concentration and Size Distribution. *Atmos. Environ*. **1978**, 12, 2439-2447.
8. Ensor, D. S.; Pilat, M. J. Calculation of Smoke Plume Opacity from Particulate Air Pollutant Properties. *J. Air Pollut. Control Assoc.* **1971**, 21, 496-501.
9. Ensor, D. S.; Pilat, M. J. The Effect of Particle Size Distribution on Light Transmittance Measurement. *An. Ind. Hyg. Assoc. (AIHA).* **1971**, May, 287-292.
10. Cowen, S. J.; Ensor, D. S.; Sparks, L. E. The Relationship of Fly Ash Light Absorption to Smoke Plume Opacity. *Atmos. Environ.* **1981**, 15, 2091-2096.

11. Steig, T. W.; Pilat, M. J. Comparison of Opacities Measured by Portable and Cross-Stack Transmissometer at a Coal-Fired Power Plant. *Atmos. Environ.* **1983**, 17, 1-9.

12. Conner, W. D.; Knapp, K. T. Relationship between the Mass Concentration and Light Attenuation of Particulate Emissions from Coal-Fired Power Plants. *J. Air Pollut. Control Assoc*. **1988**, 38, 152-157.

13. Pilat, M. J.; Ensor, D. S. Comparison between the Light Extinction Aerosol Mass Concentration Relationship of Atmospheric and Air Pollutant Emission Aerosols. *Atmos. Environ.* **1971**, 5, 209-215.

14. Srivastava, R. K.; Miller. C.A.; Erickson, C.; Jambjekar, R. Emissions of Sulfur Trioxide from Coal-Fired Power Plants. *J. Air & Waste Manage. Assoc*. **2004**, 54, 750-762.

15. Pilat, M. J.; Wilder, J. M. Opacity of Monodisperse Sulfuric Acid Aerosols. *Atmos. Environ.* **1983,** 17, 1825-1835.

16. Wilder, J.M.; Pilat, M.J. Calculated Droplet Size Distributions and Opacities of Condensed Sulfuric Acid Aerosols. *J. Air Pollut. Control Assoc*. **1983**, 33, 58-863.

17. Lou, J. C.; Lee, M.; Chen, K. S. Correlation of Plume Opacity with Particles and Sulfates from Boilers. *J. Environ. Eng*. **1997**, 123, 698-703.

18. Meng, R. Z.; Seignneur, P. C. Simulation of Stack Plume Opacity. *J. Air & Waste Manage. Assoc*. **2000**, 50, 869-874.

19. Wieprecht, W.; Stieler, M.; Heinze, G.; Moller, D.; Riebel, U.; Hoffmann, E.; Sparmann, A.; Kalab, D.; Acker, K.; Auel, R. Droplet Concentration (LWC) and its Chemical Composition after Gas Cleaning in the Lignite Fired Power Plant Janschwalde (FRG). *J. Aero. Sci.* **1998**, 29, S207-S208.

20. Goodwin, D. G.； Mitchner, M. Measurements of the Near Infrared Optical Properties of Coal Slugs. *Chem. Eng. Comm.* **1986**, 44, 241-255.
21. Boothroyd, S. A.； Jones, A. R.； Nocholson, K. W.； Wood, R. Light Scattering by Fly Ash and the Applicability of Mie Theory. *Combust. Flame*. **1987**, 69, 235-241.
22. Bohren, C. F.; Huffman, R. H. *Absorption and Scattering of Light by Small Particles*; John Wiley and Sons: New York, **1983**, p 477-482.
23. Jung, C. H.; Kim, Y. P. Particle Extinction Coefficient for Polydispersed Aerosol using a Harmonic Mean Type General Approximated Solution. *Aerosol Sci. Technol.* **2007**, 41, 994-1007.
24. Modest, M. F. Radiative Heat Transfer; Academic Press: New York, **2003**, p 363-375.
25. Van de Hulat, H. C. Light Scattering by Small Particles, John Wiley & Sons: New York, **1981**.
26. Kerker, M. The Scattering of Light and Other Electromagnetic Radiation, Academic Press, New York, **1969**.
27. Deirmendjian, D. Electromagnetic Scattering on Spherical Polydispersions, Elsevier, New York, **1969**.
28. Wylie, C.R. Advanced Engineering Mathematics, 5th ed., McGraw-Hill, New York, **1982**.
29. Abramowitz, M. and Stegun, I. A. Handbook of Mathematical Functions, Dover Publications, New York, **1965**.
30. Weir, A. Jr.; Dale, J, J.; Papey, L. T.; Seymour C.; Shin Chow Yung. Factors influencing plume opacity. *Environ, Sci. Technol.*, **1976**, 10, 539-544.

31. Laurent, S. Investigation of Plume Opacity Formation at Cement Kiln Stacks. Doctor Thesis, Swiss Federal Institute of Technology Zurich, **1999**.

32. Loh, M.H.; Beck, J.V. Simultaneous Estimation of Two Thermal Conductivity Components from Transient Two-Dimensional Experiments. In *ASME Winter Annual Meeting, Atlanta, GA, December 1-6, 1991*； American Society of Mechanical Engineers： New York, NY, **1991**； Paper 91-WA/HT-11.

33. Beck, J. V.; Arnold, K. J. Parameter Estimation in Engineering and Science, Wiley: New York, **1977**, p.17.

34. Hodkinson, J. R.; The Optical Measurement of Aerosols. C. N. Davies, Ed; Academic Press; *Aero. Sci.* New York, **1966**, 316-326.

35. Hinds, W. C. Aerosol Technology, John Wiley & Sons: New York, **1981**, p.354

36. Cho, H.; Oh, D.; Kim, K. A Study on Removal Characteristics of Heavy Metals from Aqueous Solution by Fly Ash. *J. Hazard. Mater*. **2005**, B127, 187-195.

37. Wyatt, P. J. Some Chemical, Physical, and Optical Properties of Fly Ash Particles, *Appl. Optics*, **1980**, 19, 975-983.

38. Ruan, L. M.； Qi, H.； An, W.； Tan, H. P. Inverse Radiation Problem for Determination of Optical Constants of Fly-Ash Particles. *Int. J. Thermo.* **2007**, 28, 1322-1341.

39. Gupta, R. P.； Wall, T. F.； Truelove, J. S. Radiative Scatter by Fly Ash in Pulverized Coal-Fired Furnaces: Application of the Monte Carlo Method to Anisotropic Scatter. *Int. J. Heat and Mass Transfer*. **1983**, 26, 1649-1660.

40. Gupta, R. P.； Wall, T. F. The Optical Properties of Fly Ash in Coal Fired Furnaces. *Combust. Flame*, **1985**, 61, 145-151.

41. Boothroyd, S. A.；Jones, A. R. A Comparison of Radiative Characteristics for Fly Ash and Coal. *Int. J. Heat and Mass Transfer*, **1986**, 29, 1649-1654.

42. Pilat, M. J. Optical Efficiency Factor for Concentric Spheres. *Appl. Optics,* **1967**, 6, 1555-1558.

43. Fu, X.; Viskanta, R.; Gore, J. P. A Model for the Volumetric Radiation Characteristics of Cellular Ceramics. *Int. J. Heat and Mass Transfer*, **1997**, 29, 1069-1082.

44. 台灣電力公司，通宵廠燃油機組煙氣粒狀物排放濃度與粒狀物不透光率換算關係研究，台灣電力公司, **1995**.

45. Taiwan Power Company. Taiwan Power Company Opacity Correlation Study. *Taiwan Power Company Publishers*, Taipei, Taiwan, **2005**, Chapter 5.

List of publications

1. Tu, W. F. ; Lin, J. D. ; Wu, Y. L. Effect of Boiler Loads on the Particle Extinction Coefficient at a Coal-Fired Power Plant with Flue Gas Desulfurization. 27th Annual AAAR Conference. *Aerosol Sci. Technol.* **2008**, p. 64.
2. Tu, W. F. ; Lin, J. D. ; Wu, Y. L. Investigation on Factors Influencing in-stack Plume Opacity at a Coal-fired Power Plant with Flue Gas Desulfurization. 101th Annual A&WMA Conference. *J. Air & Waste Manage. Assoc*. **2009,** p.82.
3. Tu, W. F.; Lin, J. D.; Wu, Y. L. An analysis on Extinction Coefficients of Particles and Water Moisture in the Stack after Flue Gas Desulfurization at a Coal-Fired Power Plant. *J. Air & Waste Manage. Assoc*. **2011**, 61, 815-825.